Investigation of Unsteady Flow of Micropolar Fluid over an Exponentially Stretching Sheet

By

ANAM FATIMA

NATIONAL UNIVERSITY OF MODERN LANGUAGES

ISLAMABAD

3rd August, 2024

Investigation of Unsteady Flow of Micropolar Fluid over an Exponentially Stretching Sheet

By

ANAM FATIMA

MS Mathematics, National University of Modern Languages, Islamabad, 2024

A THESIS SUBMITTED IN PARTIAL FULFILMENT OF
THE REQUIREMENTS FOR THE DEGREE OF

MASTER OF SCIENCE

In Mathematics

To

FACULTY OF ENGINEERING & COMPUTING

NATIONAL UNIVERSITY OF MODERN LANGUAGES ISLAMABAD

THESIS AND DEFENSE APPROVAL FORM

The undersigned certify that they have read the following thesis, examined the defense, are satisfied with overall exam performance, and recommend the thesis to the Faculty of Engineering and Computing for acceptance.

Thesis Title: Investigation of Unsteady flow of Micropolar fluid over an Exponentially Stretching Sheet

Submitted By: Anam Fatima **Registration #:** 62 MS/MATH/S22

Master of Science in Mathematics (MS MATHS)
Title of the Degree

Mathematics
Name of Discipline

Dr. Asia Anjum
Name of Research Supervisor

Signature of Research Supervisor

Dr. Sadia Riaz
Name of HOD

Signature of HOD

Dr. Muhammad Noman Malik
Name of Dean (FEC)

Signature of Dean (FEC)

August 3rd, 2024

AUTHOR'S DECLARATION

I Anam Fatima

Daughter of Muhammad Shafi

Registration # 62 MS/MATH/S22

Discipline Mathematics

Candidate of **Master of Science in Mathematics (MS MATHS)** at the National University of Modern Languages do hereby declare that the thesis **Investigation of Unsteady Flow of Micropolar Fluid over an Exponentially Stretching Sheet** submitted by me in partial fulfillment of MS degree, is my original work, and has not been submitted or published earlier. I also solemnly declare that it shall not, in future, be submitted by me for obtaining any other degree from this or any other university or institution. I also understand that if evidence of plagiarism is found in my thesis/dissertation at any stage, even after the award of a degree, the work may be cancelled and the degree revoked.

Signature of Candidate

Anam Fatima

Name of Candidate

3rd August, 2024

Date

ABSTRACT

Title: Investigation of Unsteady flow of Micropolar fluid over an Exponentially Stretching Sheet.

This thesis presents the investigation of unsteady flow of micropolar fluid over an exponentially stretching sheet. A system of connected nonlinear partial differential equations is turned into nonlinear ordinary differential equations by employing similarity transformations. By using HAM technique, the series solution is obtained. A brief discussion, tabulation, and drawing of the physical parameters influencing the flow and heat transfer phenomena are provided. Temperature drops significantly because of unsteadiness, and fluid velocity reduces as the unsteadiness parameter increases. The velocity field is decreases when the micropolar parameter increases. On the other hand, as the micropolar parameter increases, the temperature rises.

TABLE OF CONTENTS

LIST OF TABLES

LIST OF FIGURES

LIST OF ABBREVIATIONS

MHD	Magnetohydrodynamics
HAM	Homotopy analysis method
PDEs	Partial differential equations
ODEs	Ordinary differential equations

LIST OF SYMBOLS

u, v	Velocity component
x, y	Cartesian coordinates
$\mathrm{Cf_x}$	skin friction coefficient
$\mathrm{Re_x}$	Reynolds number
f	Dimensionless velocity
S	Unsteadiness parameter
j	Microinertia
h	Heat transfer coefficient
g	Dimensional microrotation velocity
k	Vortex viscosity
K	Micropolar parameter
N_0	Microrotation parameter
$\mathrm{N^*}$	Angular velocity
$\mathrm{Nu_x}$	Local Nusselt number
Pr	Prandtl number
$\mathrm{q_w}$	Surface heat flux
T	Temperature
$\mathrm{T_\infty}$	Ambient fluid temperature
$\mathrm{T_w}$	Temperature of the wall
$\mathrm{T_f}$	Hot fluid temperature
γ	Slip parameter
α	Thermal diffusivity
ρ	Fluid density
μ	Dynamic viscosity
Ec	Eckert number
M	Magnetic field parameter
A	Unsteadiness parameter
$\mathrm{A_1}$	Dimensionless parameter
σ	Electrical conductivity
$\mathrm{k_1}$	Thermal conductivity
$\mathrm{B_0}$	

ν	Biot number
C_p	Kinematic viscosity
n	Specific heat
&	Constant
ξ	And
τ_w	Similarity variable
f'	Share stress
θ'	Velocity profile
	Temperature profile

ACKNOWLEDGMENT

It is beyond my comprehension to express my warm appreciation to the Almighty Allah, the most merciful and beneficial being in the universe. I also express my gratitude to the last Prophet of Almighty Allah, Hazrat Muhammad (PBUH) the supreme reformer of the world and great educator for human being.

I am thankful to my father (Prof. Muhammad Shafi Tahir) and Mama for their kindness, love, supports and they have always been around me to share my achievements and successes. I would like to express my deep gratitude to my MS supervisor, Dr. Asia Anjum and my co supervisor, Dr Adnan Saeed Butt for their valuable guidance and encouragement throughout the process of writing this thesis. They left no stone unturned to guide me throughout my research journey. I would like to acknowledged all my teachers in the Department of Mathematics for their contributions to my education.

Lastly, I want to express my heartfelt gratitude to my brother (Dr Raheel Kamran), who has provided me with unwavering support throughout my MS degree journey and those people who assist me even in the minutest way possible.

(Anam Fatima)

DEDICATION

This thesis is dedicated to my parents, teachers, and brothers, who always supported and nurtured me for achieving this goal. All of them have been a source of motivation and strength during moments of despair and discouragement.

CHAPTER 1

INTRODUCTION

1.1 Micropolar Fluid

Micropolar fluids, which exhibit internal microstructural effects, allow for more complex behaviors. These fluids have degrees of freedom for both translation and rotation, enabling them to move and rotate independently. To account for these characteristics, the mathematical description of micropolar fluid dynamics incorporates additional factors, providing a more comprehensive understanding of fluid behavior. This approach is valuable in fields such as engineering, materials science, and fluid dynamics. In this study, thermodynamic principles are used as constraints to derive the field equations for density, velocity, and the microrotation vector. Additionally, equations for micropolar fluids are derived, addressing their response to micro rotational motions and spin inertia, as established by Eringen *et al*. [1].

Mathematical and computational models enhance the study of solar energy engineering in magnetic micropolar polymers. Shamshuddin *et al.* [2] revealed that material and suction/injection parameters reduce microrotation and velocity. Yasmin *et al*. [3] explored heat and mass transfer in a non-Newtonian micropolar fluid over a curved stretched sheet using magnetohydrodynamics, showing that magnetic field interactions affect temperature and concentration distribution. Mandal *et al*. [4] investigated the impact of radiation and velocity slip on the flow and melting heat transfer of a micropolar fluid, demonstrating that these factors significantly influence its properties. Patel *et al*. [5] used the Homotopy Analysis Method (HAM) to examine thermal radiation, chemical processes, and heat production in unsteady micropolar fluid flow, finding that micropolarity reduces velocity distribution, increases buoyant force, and raises temperatures.

The analysis investigated heat and mass transfer caused by slide impacts in a porous medium with permeable sheets on magnetohydrodynamic (MHD) micropolar fluids. Using MATLAB, the equations for concentration, heat, momentum, and microrotations were simplified. The findings, presented by Sharma *et al.* [6], demonstrate that micropolar fluids suppress

microrotation profiles while enhancing velocity and temperature profiles. Additionally, the thickness of the momentum boundary layer is reduced by magnetic and porosity characteristics. This work also examined the formation of entropy in stretchy sheets subjected to an unsteady flow of a reactive hydromagnetic micropolar fluid. Fatunmbi *et al.* [7] showed that velocity profiles are accelerated by micropolar material terms, whereas dimensionless concentration, temperature, and velocity profiles are degraded. Meenakumari *et al.* [8] explored Darcy-Forchheimer flow over a stretching surface by analyzing chemical reactions, heat radiation, activation energy, viscosity dissolution, Dufour, and Soret effects. The study concluded that heat radiation and Eckert numbers significantly increase temperature distribution.

1.2 Stretching Sheet

A stretching sheet is a flat surface over which a fluid flows, undergoing continuous elongation or contraction. Common industrial processes that use stretching sheets include extrusion, hot rolling, and polymer manufacturing. This research examines the flow of an incompressible second-order fluid past a stretched sheet. Rajagopal *et al*. [9] explored the impact of this phenomenon on polymer processing, specifically focusing on a polymer sheet that is continuously extruded from a die. Kumarane *et al.* [10] further investigated this topic, emphasizing mass flux and its effects on flow and streamlining patterns during incompressible viscous motion across a stretching sheet.

The study examined heat transmission over a stretching sheet and the dual solution of the two-dimensional Casson fluid magnetohydrodynamics flow under a homogeneous magnetic field. It focused on the effects of linear thermal radiation on these solutions, paying particular attention to steady and unsteady flows. Using partial differential equations and Maple 2015 simulations, Hamid *et al.* [11] revealed positive eigenvalues and numerical stability for Casson fluid flow profiles, thereby developing dual solutions. Additionally, Srinivasulu *et al.* [12] investigated the behavior of Williamson nanofluid on a stretching surface in the presence of an aligned magnetic field. This was accomplished using partial differential equations and graphical depictions of parameter values.

Using the Keller-box method and similarity transformation, Alzahrani *et al.* [13] investigated the effects of microparticle suspension on convective micropolar fluid flow over an impervious nonlinear stretching sheet. The study also analyzed a nonlinear mathematical

model of a liquid moving toward a micropolar stagnation point in a permeable, stretchable device, considering thermofluid factors affecting heat transmission, microrotation, reacting species profiles, and flow rate. The results indicated that increasing buoyancy, stretching velocity, permeability, magnetic field, viscous dissipation, and radiation all influence the micro-gyration of micropolar particles. Furthermore, the study by Ram *et al.* [14] demonstrated a growing reaction index for improved mass transfer. Additionally, the research examined the thermo-variation and flow phenomenon of a magnetized stretching sheet-induced radiative nanofluid flow using graphene nanomaterial. The findings showed that the temperature profile and concentration increase with the Biot number. The accuracy of these results was confirmed by Ali *et al*. [15].

Saidulu *et al.* [16] investigated the effects of chemical processes and viscous dissipation on the transfer of heat and mass in the hydromagnetic flow of a micropolar fluid across a stretched sheet. The flow regime equations were solved numerically using MATLAB's built-in bvp4c method. The findings indicated that velocities, temperatures, microrotations, and concentration functions are all influenced by magnetic fields. Magyari *et al*. [17] examined the similarity solutions for steady plane boundary layers on a continuously stretched surface with an exponential temperature distribution and extension. Nazar *et al*. [18] explained the constant laminar 2D boundary layer flow and heat transfer of an incompressible viscous fluid with thermal radiation over an exponentially stretched sheet. Additionally, Ishak *et al*. [19] described the impact of radiation on a viscous fluid's magnetohydrodynamic (MHD) boundary layer flow over an exponentially stretched sheet.

1.3 Exponentially Stretching Sheet

When a surface becomes longer or wider with increasing distance from a specific location, it is referred to as an exponentially extending sheet. The stretching of such a sheet can be described mathematically, where the extended dimension and a variable regulate the stretching rate. Exponentially stretched sheets serve as excellent models for examining boundary phenomena and optimizing production processes. They are widely used in many engineering and industrial processes, particularly in fluid flow and heat transfer investigations. The micropolar boundary-layer flow and heat transmission properties of an exponentially stretching heated sheet cooled by mixed convection flow were studied. This study examined how buoyancy and viscous dissipation influence the convective transport

within the boundary-layer region. Abd El-Aziz *et al.* [20] provided a graphical representation of the results.

The thermal radiation and two-dimensional, laminar, stable, and incompressible third-grade viscoelastic micropolar fluid flow over an exponentially stretched sheet were studied, focusing on how thermophoresis and Brownian motion affect nanoparticle migration in nanofluids. Awan *et al*. [21] examined various physical parameters in terms of their impacts on non-dimensional concentrations, temperatures, velocities, microrotation, and induced magnetic field profiles using dimensionless linked ordinary differential equations (ODEs) and partial differential equations (PDEs). The unique microstructures of micropolar fluids make them valuable in industrial applications. For non-Newtonian liquids, Guedri *et al.* [22] developed a micropolar flow model using the Runge-Kutta-Fehlberg method, which showed that the distributions of temperature, concentration, and velocity all increase with the parameter values.

Fatunmbi *et al.* [23] investigated the effects of buoyant force, radiation, and slip factors on the flow of a hydromagnetic dissipative micropolar fluid through an exponentially extending vertical sheet. The main parameters influencing the results include the coefficients of skin friction, temperature, velocity, and microrotation fields, which strongly correlate with existing literature. Larger parameter estimations were found to increase fluid velocity. Abbas *et al*. [24] studied the heat and mass transportation effects of a micropolar second-grade nanofluid on porous media over an exponentially stretched surface. In another study, Bakar *et al.* [25] examined heat transport, stagnation-point flow, and magnetohydrodynamics (MHD) in a micropolar fluid. They numerically solved ordinary differential equations using MATLAB software. The results demonstrated distinct phenomena between mixed convection and micropolar convection, with temperature distribution, angular velocity, and fluid velocity profiles rising with increasing radiation, magnetic, and buoyancy parameters.

Abbas *et al*. [26] investigated the flow of second-grade micropolar nanofluid across an exponentially curved Riga sheet, taking into account the effects of slip. Siddique *et al.* [27] used the boundary layer approximation, lie symmetry approach, and the bvp4c scheme to formulate the governing equations. Additionally, the study highlighted the importance of chemical reactions, thermal radiation, and slip on the flow of magnetic second-grade fluids with nanoparticle dispersion. This research is relevant for bio-inspired fuel cells and the production of nanomaterials, utilizing a bio-convection model.

1.4 Unsteady Stretching Sheet

A surface whose rate of stretching changes over time is called an unstable stretching sheet. Such surfaces are frequently modeled in fluid dynamics and heat transfer studies to understand transient phenomena that occur in boundary layer flows over time-varying surfaces. Time-dependent boundary conditions arise because the stretching function governing the sheet's motion changes mathematically with time. Unsteady stretching sheets are utilized in various industrial processes, such as coating, thin-film deposition, and polymer processing, where control mechanisms or process dynamics can alter the stretching rate. Understanding heat transfer and fluid flow over unstable stretched sheets is crucial for predicting system behavior in dynamic situations and optimizing manufacturing operations. Abd El-Aziz *et al*. [28] examined the effect of radiation on heat and fluid flow over an unstable stretched surface. They found that when boundary layer equations were reduced to ordinary differential equations, it became evident that the rate of heat transfer increased as parameters rose, particularly for larger values of A and Pr.

A stable upper branch solution was found for all parameter values when Khan *et al.* [29] investigated the buoyancy influence on heat transfer and flow in a hybrid micropolar nanofluid across a shrinking vertical flat plate. Using a homotopy analysis methodology and a PDE framework, the analysis explored the effects of nonlinear radiation on a mixed micropolar fluid. Kataria *et al.* [30] examined how different parameters affect the gradients of temperature, velocity, and concentration, noting a higher Nusselt number at elevated Prandtl number concentrations. Additionally, Abbas *et al.* [31] used mathematical models and numerical analysis to investigate magnetized micropolar fluid flow over a curved surface, revealing improved heat transmission, a decreased heat transfer rate, and a higher surface-fluid fraction.

1.5 Magnetohydrodynamics (MHD)

Magnetohydrodynamics (MHD) is a branch of fluid dynamics that examines how electrically conducting fluids, such as electrolytes, liquid metals, and plasmas, behave when exposed to magnetic fields. In MHD, electric currents are generated due to interactions between fluid motion and the magnetic field, which in turn affect the fluid flow. Understanding the behavior of conducting fluids in magnetic fields is crucial for applications across various sectors,

including engineering, fusion research, geophysics, plasma physics, and astrophysics. Jang *et al*. [32] investigated the flow of electrically conductive liquids in electric and magnetic fields and introduced a novel micropump based on MHD principles. The Lorentz force drives the conductive fluid within the microchannel. The function of the micropump is evaluated using pressure head differences and flow rates, and bubble formation is observed. The experimental results are compared with theoretical predictions.

Kumar *et al*. [33] investigated how fluid temperature increases with Eckert number, irradiation, and magnetic parameters in the context of magnetohydrodynamics (MHD) flow across a stretching sheet. The study explored the effects of viscous dissipation, heat generation, and slip conditions on MHD and micropolar fluid flow, as well as heat transfer over a stretching sheet. They found that an increase in the material parameter K reduced the velocity field. Abbas *et al*. [34] examined non-linear stretching sheets and mixed convection flow with micropolar fluid in a magnetic field, discovering that material characteristics and thermal radiation enhanced velocity profiles. Patal *et al*. [35] investigated inclined MHD micropolar fluid flow, revealing that the magnetic field induces surface friction and mass transfer, which leads to an increased Nusselt number and dual nature behavior. Additionally, Mahabaleshwar *et al*. [36] contributed to this field with further insights into these phenomena.

Mishra *et al*. [37] investigated the influence of various factors on flow variables, specifically analyzing Williamson micropolar fluid flow through a non-linearly stretched sheet under high-temperature convection. Jawad *et al*. [38] studied the magnetohydrodynamic stagnation point flow of micropolar fluid using a numerical method that accounts for buoyancy forces, thermal radiation, electrical conductivity, and non-zero mass flux. Bejawada *et al*. [39] examined heat transfer in micropolar fluid flow using magnetohydrodynamics over a moving plate. They found that the friction coefficient increased with rising values of M and n, while velocity increased with higher values of β and Gr.

1.6 Contribution to the Thesis

In this thesis, a review study of Butt *et al*. [40] has been presented. Moreover, this study provides an extension to the review study by investigating how unsteady viscous fluids pass over an exponentially stretching sheet. Through the use of similarity transformations, the governing PDEs are transformed into a system of nonlinear differential equations, which are analytically solved by the homotopy analysis method (HAM). The tables and graphs are

created using the MATHEMATICA software. The results are displayed using tables and graphs.

1.7 Thesis Organization

The content of the thesis is briefly summarized in the information below:

Chapter 1 is an introductory chapter that gives a quick analysis of the key ideas, a summary of the literature on micropolar fluids, the contributions made by the thesis, and how it is organized.

Chapter 2 gives definitions, rules, and concepts that are vital to the execution of future work. On the last page of this chapter, there is a description of the homotopy analysis method.

Chapter 3 provides a thorough analysis of the work done by Butt *et al*. [40] and simulates baseline work for comparison.

Chapter 4 displays the extended work of Butt *et al*. [40]. The flow of unsteady flow of micropolar fluid over an exponentially stretching sheet is investigated. Homotopy analysis method is used to solve the governing similarity transformations. Graphs and tables are used to discuss the results for different parameters.

Chapter 5 concludes this thesis and identifies the direction for further research.

References A bibliography for this work is provided at the end.

CHAPTER 2

BASIC DEFINITIONS AND EQUATIONS

2.1 Fluid

A fluid, which can be either a liquid or a gas, is a substance that cannot withstand shear forces. When an exterior force is applied, it will first slightly resist the external shearing force before continuing to move and change. Liquids, gases, and plasmas are some of its examples.

2.2 Fluid Mechanics

The area of applied mathematics that examines fluid dynamics, characteristics, and forces acting on them. There are two primary branches:

2.2.1 Fluid Dynamics

The area of fluid mechanics concerned with force and its impact on the characteristics of flowing fluids. Hydrodynamics and aerodynamics are examples of fluid dynamics.

2.2.2 Fluid Statics

The branch of fluid mechanics that deals with the description of properties of stationary fluids. Hydrostatic pressure, buoyancy and dam design are examples of fluid statics.

2.3 Types of Flow

2.3.1 Steady Flow

The term "steady flow" describes a fluid's characteristics being steady over time, such as a river's steady flow rate, guaranteeing that the water's characteristics don't alter.

2.3.2 Unsteady Flow

Unsteady flow is the term used to describe fluid characteristics that dynamically alter over time, producing abrupt variations in pressure and velocity that resemble a sudden river surge.

2.3.3 Laminar Flow

Laminar flow, which can occur in a variety of ways, is the ordered, smooth motion of molecules of fluid in small pipelines, frequently at high viscosity and low velocity.

2.3.4 Turbulent Flow

Large-diameter pipelines with turbulent flow are frequently studied using fluid dynamics analysis, which uses algorithms and numerical analysis to identify different types of flow and reduce energy loss. For example, oil and gas pipeline optimization.

2.3.5 Incompressible Flow

Fluid density stays constant in incompressible flow, meaning that volume doesn't change regardless of changes in pressure or temperature. For example, urban water distribution system.

2.3.6 Compressible Flow

Compressible flow, which is defined as a fluid's density changing as a result of pressure and temperature changes, is important for applications such as aerodynamics, which supersonic &

hypersonic flows, as well as other high-speed scenarios involving large pressure and speed changes.

2.3.7 Transient Flow

In the context of fluid dynamics, transient flow describes fluid motion in which variables such as pressure and velocity vary over time, representing dynamic shifts that occur under sudden system circumstances or startup events. It is essential to comprehend this for system stability and engineering prediction. For example, water hammer in pipeline system.

2.4 Types of Fluid

2.4.1 Newtonian Fluid

The fluid that obeys the "Newton's law of viscosity" refers to Newtonian fluids.
Mathematically,

$$\tau \propto \frac{du}{dy}, \quad \text{or} \quad \tau = \mu \frac{du}{dy}, \tag{2.1}$$

where μ is the absolute or dynamic viscosity, also referred to as the proportionality constant, and τ is the shear stress applied to the fluid element. Navier-Stokes equations are used to represent the fluid's motion. The following relation is satisfied by the Cauchy stress tensor **T** for Newtonian fluids.

$$\boldsymbol{T} = -p\boldsymbol{I} + \boldsymbol{A_1}, \tag{2.2}$$

where p for hydrostatic pressure, $\boldsymbol{I}$ stands for identity tensor, $\boldsymbol{A_1}$ for first Rivlin-Ericksen tensor, and μ for fluid dynamic viscosity:

$$\boldsymbol{A_1} = grad\boldsymbol{V} + (grad\boldsymbol{V})^T, \tag{2.3}$$

where $\boldsymbol{V}$ is the velocity.

2.4.2 Non Newtonian Fluid

The Fluid that doesn't obey the "Newton's law of viscosity" refers to non Newtonian fluid.
Mathematically,

$$\text{Shear Stress} = k\left(\frac{dV}{dy}\right)^{n},\ n \neq 1 \tag{2.4}$$

where k is consistency index and n is the flow behavior index.

2.5 Micropolar Fluids

A micro-polar fluid is a kind of fluid that permits its constituent particles to have both translational and rotational degrees of freedom due to internal micro structural influences. Examples are biological fluids and colloidal suspensions, which display intricate behaviors not covered by traditional fluid dynamics.

2.6 Heat Source

A spacecraft's interior or exterior heat sources, such as internal electrical or propulsion systems, friction from moving elements, or sunlight, all contribute to the spacecraft's temperature rise. Gases, atmospheres, and planets are a few examples.
The following lists the three important forms of heat flow:

2.6.1 Convection

Convection, a natural phenomenon that involves molecules moving from hot to cold, has a big impact on the weather, industrial processes, cookery, and climate in a lot of different ways.

2.6.2 Conduction

Heat is transferred through conduction, which mostly occurs in liquids and solids when electrons or molecules interact. Close-knit materials, such as frying pans with protected handles for improved conductivity, have the maximum efficacy.

2.6.3 Mixed Convection

A type of heat transfer in which fluid flow contains both forced and natural convection. Applications include electronic cooling systems and heat exchangers.

2.6.4 Forced Convection

One sort of heat transfer known as forced convection occurs when an external device, such as a pump, forces a fluid to move through a channel or over a surface. This procedure, which speeds up fluid flow, is frequently employed in technical applications such as heating, cooling, and combustion engines.

2.6.5 Free Convection

Due to temperature changes, free convection, a kind of heat transport in fluids, is essential in applications in engineering like cooling structures, exchangers for heat, and electronic device performance.

2.6.6 Radiation

The term "radiation" describes the process by which heat is transferred by infrared radiation, which is energy that a material releases as electromagnetic radiation or particles. It can come from man-made sources like nuclear power plants and medical X-rays, or natural sources like cosmic radiation from space or radioactive materials. Elevated radiation exposure can cause harm to living organisms and raise the danger of radiation sickness and cancer.

2.7 Thermal Conductivity

Thermal conductivity is a property of a material that indicates how well it conducts heat. Mathematically,

$$k = \frac{Q \times L}{A \times \Delta T}. \tag{2.5}$$

So,

$$\text{Thermal conductivity} = \frac{\text{distance} \times \text{heat}}{\text{temprature gradient} \times \text{area}}, \tag{2.6}$$

where Q is the heat flow per unit time, k stands for heat conductivity, ΔT for temperature difference, and A is denoted for cross sectional area.

2.8 Thermal Diffusivity

Thermal diffusivity is the product of density and specific heat capacity divided by thermal conductivity, and it measures how quickly heat diffuses through a material in relation to its heat storage capacity. Mathematically,

$$\alpha = \frac{k}{\rho c_p}, \tag{2.7}$$

where ρ represents the density, c_p is specific heat capacity and k is thermal conductivity.

2.9 Dimensionless Parameters

2.9.1 Prandtl Number (Pr)

The fluid viscosity, or Prandtl number, reveals the dominance of thermal diffusivity, while the thickness of the boundary layer is strongly influenced by momentum diffusivity. Mathematically,

$$\text{prandtl number} = \frac{\text{kinematic viscosity}}{\text{thermal diffusivity}}, \tag{2.8}$$

or

$$pr = \frac{\nu}{\alpha_f} = \frac{\frac{\mu}{\rho}}{\frac{k}{\rho c_p}} = \frac{\mu c_p}{k}, \tag{2.9}$$

where k for thermal conductivity, c_p for specific heat, α_f for thermal diffusivity, ν is for kinematic viscosity.

2.9.2 Eckert Number (Ec)

The fluid's kinetic energy to enthalpy difference is expressed as a dimensionless number in fluid dynamics, known as the Eckert number. It is frequently used to find out how heat transfer affects fluid flow and to characterize compressible fluids, as those in supersonic flow. Mathematically,

$$Ec = \frac{u^2}{c_p \Delta T}, \tag{2.10}$$

where c_p is specific heat capacity,u is velocity for fluid, T is the temperature of the fluid.

2.9.3 Nusselt Number (Nu)

A dimensionless metric known as the Nusselt number is used to quantify the relationship between convective and conductive heat transfer across boundaries. Mathematically,

$$Nu = \frac{h\Delta T}{k\Delta T/L} = \frac{hL}{k}, \tag{2.11}$$

where h is connective heat transfer, and L is characteristic length.

2.10 Unsteadiness Parameter

In fluid dynamics, the unsteadiness parameter, which is usually stated as the ratio of characteristic time scales, such as frequency to flow velocity or length scale, assesses the relative importance of time-varying effects in relation to other flow characteristics.

2.11 Skin friction Coefficient (C_f)

The type of friction produced when a fluid moves in relation to a solid surface is referred to as skin friction. Mathematically,

$$C_f = \frac{\tau_w}{\frac{1}{2}\rho {U_w}^2}, \tag{2.12}$$

where τ_w is the shear stress at the wall, U_w is surface velocity, and ρ represents density.

2.12 Homotopy Analysis Method (HAM)

The homotopy analysis methodology (HAM) is a useful technique for solving very nonlinear differential equations analytically. Since it guarantees the convergence of the intended solution, many academics accept this approach, which originated by Liao (1992).
The differential equation can be used to demonstrate the HAM.

$$N[\hat{w}(x)] = 0, \tag{2.13}$$

where $\hat{w}(x)$ represents unknown function, x is denoted for the independent variable, and N is denoted for a nonlinear operator. The following is the equation for zeroth order deformation.

$$(1-r)\mathcal{L}[\hat{w}(x;r) - w_0(x)] = rhN[\hat{w}(x;r)]. \tag{2.14}$$

Here L is represented as auxiliary linear operator, the symbol for the embedding parameter is r, and its values range from 0 to 1. $\widehat{w}(x;r)$ is considered as unknown function, $w_0(x)$ stands for initial approximation and h is noted as non zero auxiliary parameter.

Equation corresponding to $r = 0$ and $r = 1$ are as follows;

$$\widehat{w}(x;0) = w_0(x), \quad \text{and} \quad \widehat{w}(x;1) = w(x). \tag{2.15}$$

The ultimate solution $r(x)$ is obtained by converting r from 0 to 1, which changes the solution $\widehat{w}(x;r)$ from the initial approximation $w_0(x)$. Taylor's series expansion leads to the following expressions

$$\widehat{w}(x;r) = w_0(x) + \sum_{n=1}^{\infty} w_n(x) r^n, \quad w_n(x) = \frac{1}{n!} \frac{\partial^n \widehat{w}(x;r)}{\partial r^n}\Big|_{r=0}. \tag{2.16}$$

If $r = 1$, then

$$w(x) = w_0(x) + \sum_{n=1}^{\infty} w_n(x). \tag{2.17}$$

We get the following n order deformation equation by dividing the resultant equation by $n!$ and differentiating n times the Zeroth order deformation equation with respect to r, and setting $r = 0$, we obtain

$$\mathcal{L}[w_n(x) - \chi_n w_{n-1}(x)] = h\mathcal{R}_n, \tag{2.18}$$

$$\mathcal{R}_n(x) = \frac{1}{(n-1)!} \frac{\partial^n N[\widehat{w}(x;r)]}{\partial r^n}\Big|_{r=0}, \tag{2.19}$$

where

$$\chi_n = \begin{cases} 0, & n \leq 1 \\ 1, & n > 1 \end{cases}. \tag{2.20}$$

CHAPTER 3

Study of Entropy Generation with Multi-slip Effects in MHD Unsteady Flow of Viscous Fluid past an Exponentially Stretching Sheet

3.1 Introduction

In this chapter, an exponentially stretched sheet is investigated for an unsteady hydromagnetic slip flow of viscous fluid. The governing partial differential equations are converted into a system of non-linear differential equations using adjacent similarity variables. These equations are then analytically solved using the homotopy analysis method (HAM). A brief discussion of the effects of the physical characteristics influencing the flow and transfer of heat phenomena are provided through tables and graphs. This chapter provides a detailed review of the research paper Butt *et al*. [40].

3.2 Geometry of the problem

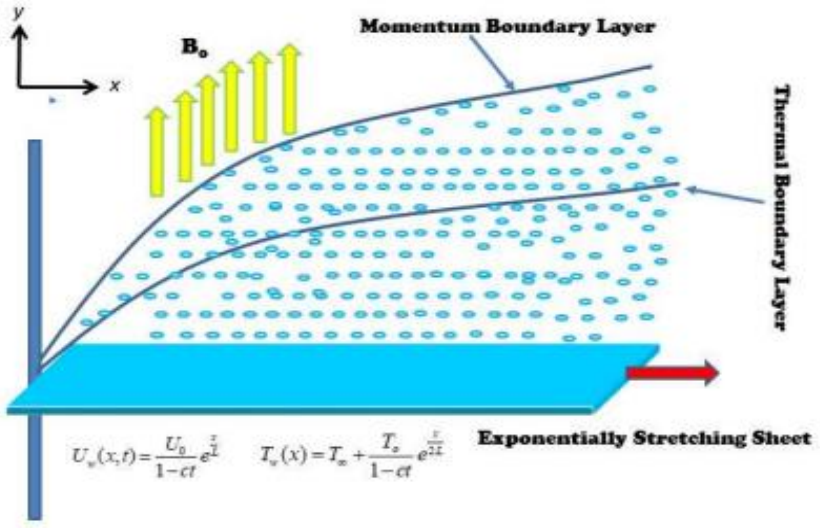

Fig 3.1. Geometry of the problem

3.3 Mathematical Formulation:

The incompressible, unsteady two dimensional flow of an electrically conducting viscous fluid is caused by an exponentially stretched surface, as seen in Fig. 3.1. The exponentially stretching surface is considered to be orientated along the x-axis, with the y-axis being normal to the surface. The region where $y \geq 0$ is assumed to contain the viscous fluid. On the surface where B_0 is the constant, a normal magnetic field with strength $B(x,t) = \frac{B_0}{\sqrt{(1-ct)}} e^{x/L}$ is applied. In this case, L stands for the characteristics length, and c is the dimensional constant. Since the magnetic Reynolds number is low, the effects of the induced magnetic field are ignored. The surface temperature is maintained at $T_w(x) = T_\infty + \frac{T_0}{(1-ct)} e^{x/2L}$ while the surface is stretched with the exponential velocity $U_w(x,t) = \frac{U_0}{((1-ct)} e^{x/L}$. It is assumed that T_∞ is the ambient temperature of the fluid. The existence of viscous and joule dissipation effects is assumed. The velocity pattern of the boundary layer flow is determined as follow:

$$\boldsymbol{V} = [u(x,y), v(x,y), 0]. \tag{3.1}$$

The continuity, momentum and energy equations are given below;

$$\boldsymbol{\nabla}.\boldsymbol{V} = 0, \tag{3.2}$$

$$\rho \frac{d\boldsymbol{V}}{dt} + \rho(\boldsymbol{V} \cdot \boldsymbol{\nabla})\boldsymbol{V} = -\boldsymbol{\nabla} P + \mu \boldsymbol{\nabla^2 V} + (\boldsymbol{J} \times \boldsymbol{B}), \tag{3.3}$$

$$\rho c_p \frac{dT}{dt} = -\text{div}\mathbf{q} + \boldsymbol{\tau}.\mathbf{L}. \tag{3.4}$$

where

$$\boldsymbol{q} = -k grad T. \tag{3.5}$$

The Cauchy stress tensor $\boldsymbol{\tau}$ is defined as;

$$\boldsymbol{\tau} = -p\boldsymbol{I} + \mu \boldsymbol{A_1}, \tag{3.6}$$

Where ρ is density of fluid, c_p is specific heat capacity, $\frac{d}{dt}$ is material derivative, $\boldsymbol{L}$ is velocity gradient, $\boldsymbol{I}$ is thermal conductivity, $\boldsymbol{q}$ is heat flux, T is fluid's temperature, $\boldsymbol{V}$ is velocity profile, and $\boldsymbol{A_1}$ first Rivilin-Erickson tensor which is given by;

$$\boldsymbol{A_1} = \boldsymbol{L} + \boldsymbol{L}^T. \tag{3.7}$$

From Eq. (3.1), we obtain

$$\boldsymbol{L} = grad\,\boldsymbol{V} = \begin{bmatrix} \frac{\partial u}{\partial x} & \frac{\partial u}{\partial y} & 0 \\ \frac{\partial v}{\partial x} & \frac{\partial v}{\partial y} & 0 \\ 0 & 0 & 0 \end{bmatrix} \text{ and } \boldsymbol{L}^T = (grad\,\boldsymbol{V})^T = \begin{bmatrix} \frac{\partial u}{\partial x} & \frac{\partial v}{\partial x} & 0 \\ \frac{\partial u}{\partial y} & \frac{\partial v}{\partial y} & 0 \\ 0 & 0 & 0 \end{bmatrix}, \tag{3.8}$$

$$\boldsymbol{A_1} = \begin{bmatrix} 2\frac{\partial u}{\partial x} & \frac{\partial u}{\partial y} + \frac{\partial v}{\partial x} & 0 \\ \frac{\partial v}{\partial x} + \frac{\partial u}{\partial y} & 2\frac{\partial v}{\partial y} & 0 \\ 0 & 0 & 0 \end{bmatrix}. \tag{3.9}$$

The component form of governing equation is defined below;

$$\frac{\partial u}{\partial x} + \frac{\partial v}{\partial y} = 0, \tag{3.10}$$

$$\frac{\partial u}{\partial t} + u\frac{\partial u}{\partial x} + v\frac{\partial u}{\partial y} = \nu\frac{\partial^2 u}{\partial y^2} - \frac{\sigma {B_0}^2}{\rho}u, \tag{3.11}$$

$$\frac{\partial T}{\partial t} + u\frac{\partial T}{\partial x} + v\frac{\partial T}{\partial y} = \frac{k}{\rho c_p}\frac{\partial^2 T}{\partial y^2} + \frac{\nu}{c_p}\left(\frac{\partial u}{\partial y}\right)^2 + \frac{\sigma B^2}{\rho c_p}u^2, \tag{3.12}$$

The appropriate boundary conditions are;

$$\left.\begin{array}{c} u = u_w(x,t) = \frac{u_0}{(1-ct)}e^{\frac{x}{l}} + \alpha\frac{\partial u}{\partial y}, v = 0,\ T = T_w(x,t) = T_\infty + \frac{T_0}{(1-ct)}e^{\frac{A_0 x}{2L}}\ at\ y = 0, \\ u \to 0, v \to 0, T \to T_\infty\ as\ y \to \infty. \end{array}\right\} \tag{3.13}$$

Here, the velocity components in the (x, y) directions are denoted by (u, v), respectively. The variables T, ν, ρ, k, σ, and c_p denote the temperature, kinematic viscosity, conductivity, thermal conductivity, electrical conductivity and specific heat constant temperature, respectively. T_0 is the reference temperature of fluid, while T_∞ is the temperature for away from the surface. The hydrodynamic slip parameter is represented by α, A_0 is the dimensional constant temperature, the reference velocity is U_0 and c is the constant with $ct < 1$ to indicate the reference temperature.The non-dimensionalized Eqs. (3.10)–(3.12) are solved using the set of similarity transformations that follow:

$$\left.\begin{aligned} u = \frac{u_0}{1-ct} e^{x/L} f'(\xi), v = -\sqrt{\frac{U_0}{2L(1-ct)}} e^{x/2L}[f(\xi) + \xi f'(\xi)], \\ \xi = \sqrt{\frac{U_0 v}{2\nu(1-ct)}} e^{x/2L} y, \qquad \theta(\xi) = \frac{T-T_\infty}{T_w-T_\infty}. \end{aligned}\right\} \tag{3.14}$$

By substituting Eq. (3.14) into Eqs. (3.10)-(3.12), the continuity Eq. (3.10) is identically satisfied, and Eqs. (3.11) and (3.12) take the following form:

$$f'' + ff' - 2f'^2 - A(\xi f' + 2f') - Mf' = 0, \tag{3.15}$$

$$\theta' + Prf\theta' - A_0 Prf'\theta - APr(4\theta + \xi\theta') + PrEcf''^2 + MPrEcf'^2 = 0. \tag{3.16}$$

After utilizing Eq. (3.14), the related boundary conditions have the following form;

$$\left.\begin{aligned} f(0) = 0, f'(0) = 1 + \gamma f''(0), \theta(0) = 1, \\ f'(\xi) \to 0, \theta(\xi) \to 0 \; as \; \xi \to \infty. \end{aligned}\right\} \tag{3.17}$$

Here, $A = \frac{CLe^{-X}}{U_0}$ is the unsteadiness parameter, $M = \frac{2\sigma {B_0}^2 L}{\rho U_0}$ denotes the magnetic field parameter, $X = \frac{x}{L}$ is the dimensionless parameter, $Pr = \frac{uC_p}{k}$is the prandtl number, $\gamma = \alpha\sqrt{\frac{U_0 e^X}{2VL(1-ct)}}$ is slip parameter, and $Ec = \frac{{U_w}^2}{C_p(T_w-T_\infty)}$ is the Eckert number. The local Nusselt number Nu_x and the skin friction coefficient Cf_x are explained as:

$$Cf_x = \frac{\tau_w|_{y=o}}{\rho {u^2}_w}, \qquad Nu_x = \frac{xq_w|_{y=o}}{k((T_w-T_\infty))}, \tag{3.18}$$

where the heat flux q_w at the surface and the shear stress τ_w are stated as

$$\tau_w = \mu\left(\frac{\partial u}{\partial y}\right)\Big|_{y=0}, \quad q_w = -k\left(\frac{\partial T}{\partial y}\right)\Big|_{y=0}. \tag{3.19}$$

The local Nusselt number Nu_x and the dimensionless form of the skin friction coefficient Cf_x can be obtained by using Eq. (3.14) and putting Eq. (3.19) into Eq. (3.18):

$$Re_x{}^{1/2}Cf_x = f''(0), \sqrt{\frac{2}{X}}Re_x{}^{1/2}Nu_x = -\theta'(0), \tag{3.20}$$

where $Re_x = \frac{U_w x}{v}$ is the local Reynolds number.

3.4 Solution Methodology

3.4.1 Homotopy Analysis Method

The homotopy analysis method (HAM) is an analytical methodology that is useful for solving high nonlinear equations. This technique has been used to solve fluid dynamics & heat transmission-related issues. Using the boundary conditions from Eq. (3.17), the HAM in this article solved Eqs. (3.15) and (3.16) by taking into account the subsequent linear operators with linear guesses;

$$\left.\begin{aligned} f_0(\xi) &= \tfrac{1}{1+\gamma}\left(1 - e^{-\xi}\right), \\ \theta_0(\xi) &= e^{-\xi}. \end{aligned}\right\} \tag{3.21}$$

and

$$\left.\begin{aligned} \mathcal{L}_f(f) &= \frac{d^3 f}{d\xi f} - \frac{df}{d\xi}, \\ \mathcal{L}_\theta(\theta) &= \frac{d^2\theta}{d\xi^2} - \theta. \end{aligned}\right\} \tag{3.22}$$

The following attributes belong to the operator mentioned above:

$$\left.\begin{aligned} \mathcal{L}_f\left(C_1 + C_2 e^{\xi} + C_3 e^{-\xi}\right) &= 0, \\ \mathcal{L}_\theta\left(C_4 e^{\xi} + C_5 e^{-\xi}\right) &= 0, \end{aligned}\right\} \tag{3.23}$$

where $Cj's, (j = 1,2, \ldots 5)$ are arbitrary constants.

The following is an expression for the zeroth order deformation problem:

$$(1-q)\mathcal{L}_f[\bar{F}(\xi;q)-f_0(\xi)]=h_f q\mathcal{N}_f[\bar{F}(\xi;q)], \tag{3.24}$$

$$(1-q)\mathcal{L}_\theta[\bar{\Theta}(\xi;q)-\theta_0(\xi)]=h_\theta q\mathcal{N}_\theta[\bar{F}(\xi;q),\bar{\Theta}(\xi;q)], \tag{3.25}$$

with

$$\left.\begin{aligned}\bar{F}(0;q)=0,&\frac{\partial\bar{F}(0;q)}{\partial\xi}=1+\gamma\frac{\partial^2\bar{F}(0;q)}{\partial\xi^2},\bar{\Theta}(0;q)=1,\\&\frac{\partial\bar{F}(\infty;q)}{\partial\xi}=0,\ \ \bar{\Theta}(\infty;q)=0.\end{aligned}\right\} \tag{3.26}$$

In this case, $q\epsilon[0,1]$ indicates the embedding parameter associated with the deformation mappings $\bar{F}(\xi;q),\bar{\Theta}(\xi;q)$ that continuously deform from $f_0(\xi)$, $\theta_0(\xi)$ to $f(\xi),\theta(\xi)$ when q varies from 0 to 1. The convergence control parameters are represented by h_f and h_θ.
The following defines the non-linear operators:

$$\left.\begin{aligned}\mathcal{N}_f[\bar{F}(\xi;q)]=&\frac{\partial^3\bar{F}(\xi;q)}{\partial\xi^3}+\bar{F}(\xi;q)\frac{\partial^2\bar{F}(\xi;q)}{\partial\xi^2}-2\left(\frac{\partial\bar{F}(\xi;q)}{\partial\xi}\right)^2\\&-A\left(\xi\frac{\partial^2\bar{F}(\xi;q)}{\partial\xi^2}+2\frac{\partial\bar{F}(\xi;q)}{\partial\xi}\right)-M\frac{\partial\bar{F}(\xi;q)}{\partial\xi},\end{aligned}\right\} \tag{3.27}$$

$$\left.\begin{aligned}\mathcal{N}_\theta[\bar{F}(\xi;q),\bar{\Theta}(\xi;q)]=&\frac{\partial^2\bar{\Theta}(\xi;q)}{\partial\xi^2}+Pr\bar{F}(\xi;q)\frac{\partial\bar{\Theta}(\xi;q)}{\partial\xi}-A_oPr\frac{\bar{F}(\xi;q)}{\partial\xi}\bar{\Theta}(\xi;q)\\&-APr\left(4\bar{\Theta}(\xi;q)+\xi\frac{\partial\bar{\Theta}(\xi;q)}{\partial\xi}\right)+PrEc\left(\frac{\partial^2\bar{F}(\xi;q)}{\partial\xi^2}\right)^2+MPrEc\left(\frac{\partial\bar{F}(\xi;q)}{\partial\xi}\right),^2\end{aligned}\right\} \tag{3.28}$$

The remaining procedure specifics are available in the literature. The following can be expressed as an infinite series to represent the solution of the differential Eqs. (3.15) and (3.16) with the constraints on the boundaries of Eq. (3.17):

$$\left.\begin{aligned}f(\xi)=f_0(\xi)+\textstyle\sum_{m=1}^{\infty}f_m(\xi),\\\theta(\xi)=\theta_0(\xi)\textstyle\sum_{m=1}^{\infty}\theta_m(\xi),\end{aligned}\right\} \tag{3.29}$$

It is evident from the preceding process that the convergence control parameters h_f and h_θ, which are contained in the series solutions indicated in Eq. (3.29), can be adjusted to regulate how quickly the series solutions converge. In order to ensure that these series solutions rapidly converge, the ideal values of h_f and h_θ were employed.

3.5 Convergence of Solution

The convergence rate was significantly increased by using a Padé approximation on the series solutions produced by the homotopy method. For the $[m/m]$ homotopy Padé approximation, Table. 3.1 exhibits the convergence of the numerical values of $-f''(0)$ and $-\theta'(0)$ when $h_f = -0.314784$, $h_\theta = -0.398461$, $M = 1.0$, $\gamma = 0.5$, $A = 1.0$, $A_0 = 0.5$, $Pr = 1.0$, $Ec = 0.2$. It is evident that at the $[15/15]$ homotopy Padé approximation, the convergence of the series solutions of Eq. (3.29) was reached up to five decimal places.

Table 3.1.

Convergence table for the $[m/m]$ homotopy Padé approximation of $-f''(0)$ and $-\theta'(0)$ when $h_f = -0.314784$, $h_\theta = -0.398461$, $M = 1.0$, $\gamma = 0.5$, $A = 1.0$, $A_0 = 0.5$, $Pr = 1.0$, $Ec = 0.2$.

$[m/m]$	$-f''(0)$	$-\theta'(0)$
[2/2]	0.9551736	1.916137
[4/4]	0.9590946	1.929443
[6/6]	0.9591626	1.929032
[8/8]	0.9591697	1.929027
[10/10]	0.9592271	1.929035
[12/12]	0.9592056	1.929040
[14/14]	0.9592039	1.929043
[16/16]	0.9592037	1.929044
[18/18]	0.9592037	1.929044
[20/20]	0.9592037	1.929044

3.6 Results and Discussion:

Under limited circumstances, the solutions to the nonlinear ordinary differential Eqs. (3.15) and (3.16) with the boundary restrictions of Eq. (3.17) were compared to the body of exciting literature. Table. 3.2 was created in order to compare the numerical values of $-\theta'(0)$ with those that were stated for various values of Pr and M when $\gamma = 0.0$, $A = 0.0$, $A_0 = 1.0$, $Ec = 0.0$, by Magyari and Keller [17], El-Aziz [20], Nazar [18], and Ishak [19]. It was observed that the HAM in the current investigation was in consistent accord with the literature. The purpose of Table. 3.2 was to observe how the factors γ, M, and A affected the dimensionless skin friction coefficient $-f''(0)$.

Fig. 3.2a–c explains how the parameters M, γ, and A affect the velocity profile $f'(\xi)$. Velocity $f'(\xi)$ decreased as a result of the strong Lorentz force opposing the fluid's motion as the strength of the magnetic field parameter M raised. In addition, the velocity $f'(\xi)$ decreased with increasing distance ξ and reached a maximum value at the exponentially stretched surface for fixed M. Asymptotically, the velocity was zero in the far away regime. Fig. 3.2.b. illustrates how the slip parameter γ affects the fluid velocity $f'(\xi)$. As the slip parameter γ increased, there was a corresponding decrease in velocity, which was consistent with the observed physical phenomenon. For modification in the unsteadiness parameter A, the velocity profile $f'(\xi)$ is plotted against ξ in Fig. 3.2.c. The graph makes clear that a decrease in velocity $f'(\xi)$ follows an increase in the unsteadiness parameter A. Thus, the momentum boundary layer thickness was less affected by the unsteadiness parameter A. The temperature distribution $\theta(\xi)$ is displayed against different flow parameters in Figs. 3.3. and 3.4. Variations in the magnetic field parameter M have an effect on $\theta(\xi)$, as seen in Fig. 3.3a. The temperature $\theta(\xi)$ rises as the value of M increases because the resistive force grows stronger. As a function of the slip parameter γ, Fig. 3.3.b. plots the temperature distribution $\theta(\xi)$. The fluid temperature was seen to increase with increasing values of γ. The behaviour of the fluid temperature is shown in Fig.3.3.c. by the manipulation of the unsteadiness parameter A values. Increasing the values of A resulted in a notable decrease in temperature. Fig. 3.4.a. shows how the temperature exponent A_0 affect $\theta(\xi)$. As the value of A_0 increased, there was a minute boost in fluid temperature. On the other hand, this boost was negligible in comparison to the temperature variation for other flow parameters. The effects of Pr on the temperature distribution $\theta(\xi)$ are shown in Fig. 3.4.b. A growing Pr value was associated with a decrease in the thickness of the thermal boundary

layer. However, Fig. 3.4.c. demonstrates that as Ec values increased, the effect of viscous dissipation were amplified, leading to an increase in fluid temperature.

Table 3.2: Comparison of current values of $-\theta'(0)$ for variations in the Prandtl number Pr and the magnetic field parameter M when $\gamma = 0.0$, $A = 0.0$, $A_0 = 1.0$, $Ec = 0.0$ with those given by Ishak [19], Nazar [18], El-Aziz [20], and Magyari and Keller [17].

M	Pr	$-\boldsymbol{\theta'(0)}$ Magyari and Keller [17]	$-\boldsymbol{\theta'(0)}$ E1-Aziz [20]	$-\boldsymbol{\theta'(0)}$ Bidin and Nazar [18]	$-\boldsymbol{\theta'(0)}$ Anuar Ishak [19]	Present $-\boldsymbol{\theta'(0)}$ HAM
0.0	1.0	0.954782	0.954785	0.9548	0.9548	0.95478
	2.0			1.4714	1.4715	1.47146
	3.0	1.869075	1.869072		1.8691	1.86907
	5.0	2.500135	2.500132		2.5001	2.50012
	10.0	3.660379	3.660372		3.6604	3.66027
1.0	1.0				0.8611	0.86109

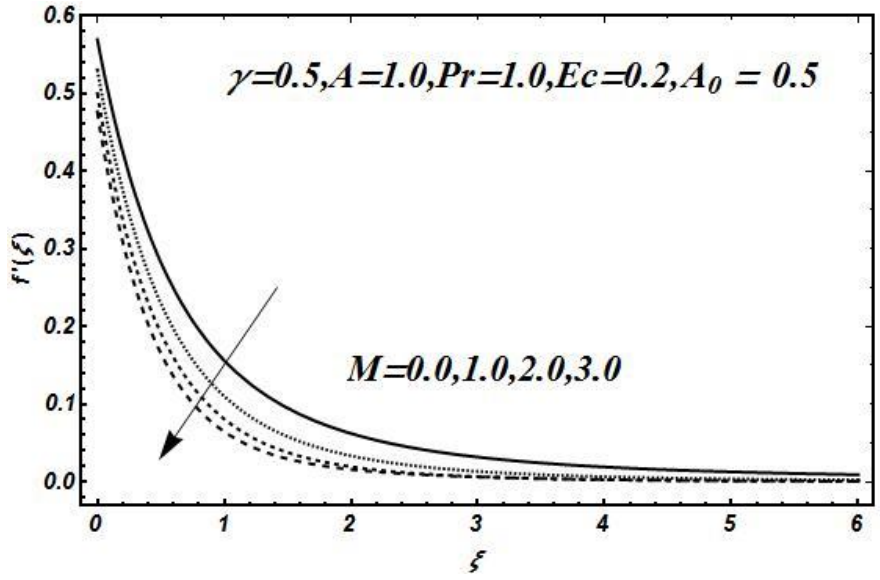

Fig. 3.2. a. Effect of the magnetic field parameter M on the velocity profile $f'(\xi)$.

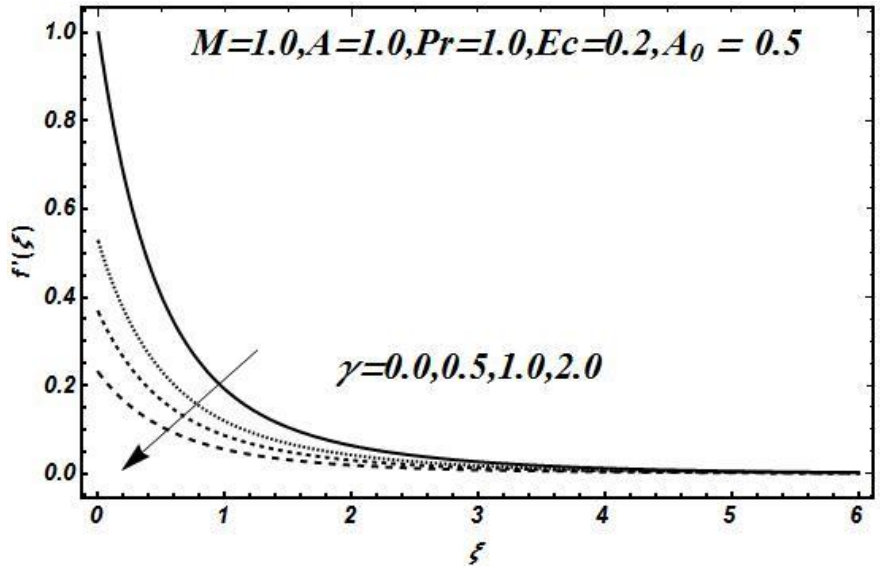

Fig 3.2. b. Effect of slip parameter γ on velocity profile $f'(\xi)$.

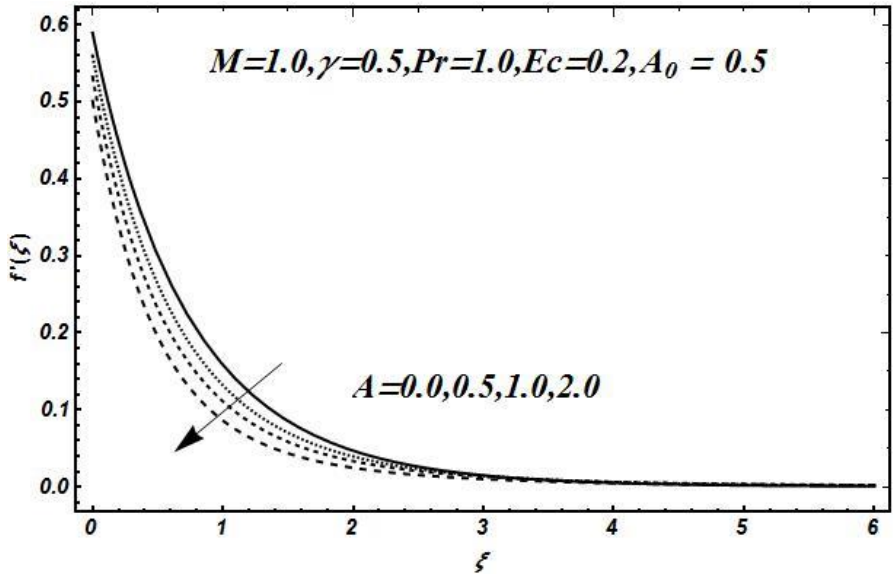

Fig. 3.2. c. Effect of unsteadiness parameter A on velocity profile $f'(\xi)$.

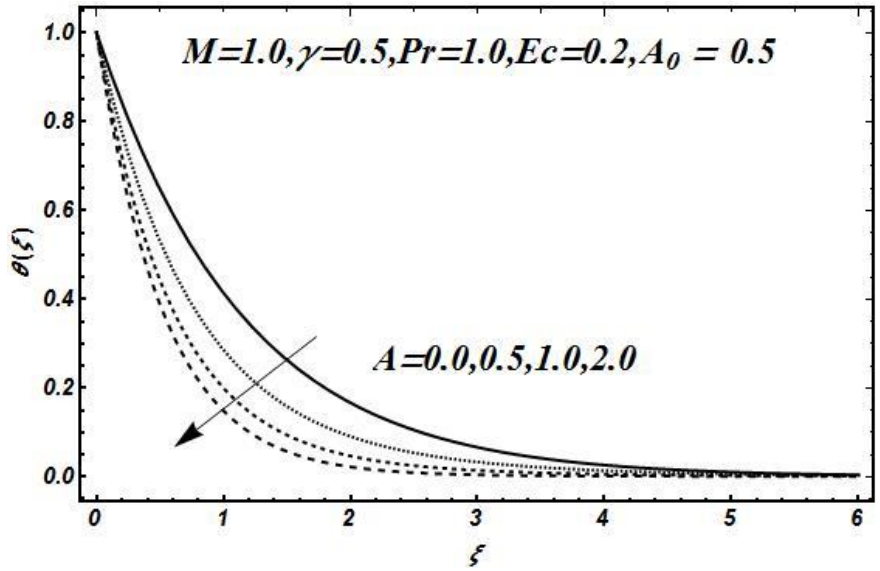

Fig. 3.3. a. Effects of the unsteadiness parameter A on the $\theta(\xi)$.

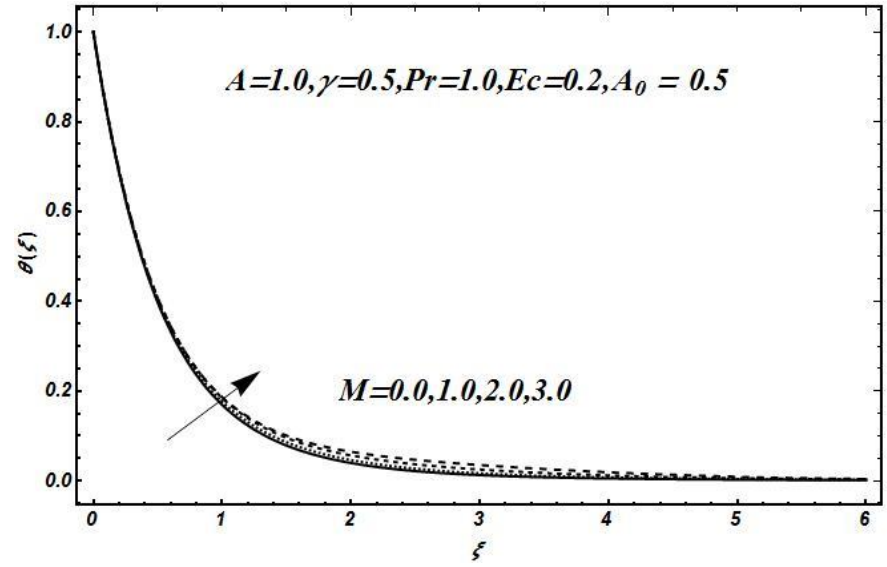

Fig. 3.3. b. Effects of the magnetic field parameter M on the $\theta(\xi)$.

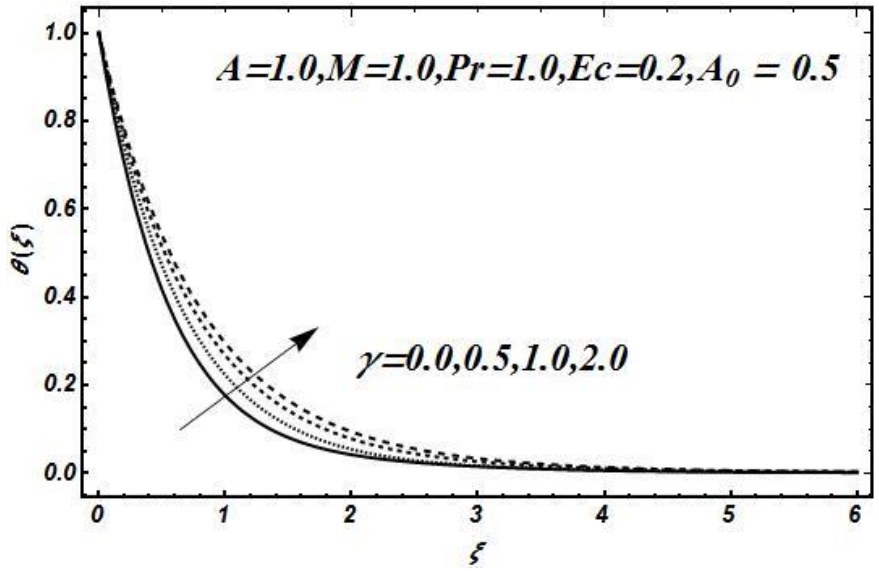

Fig. 3.3. c. Effects of the slip parameter γ on the $\theta(\xi)$.

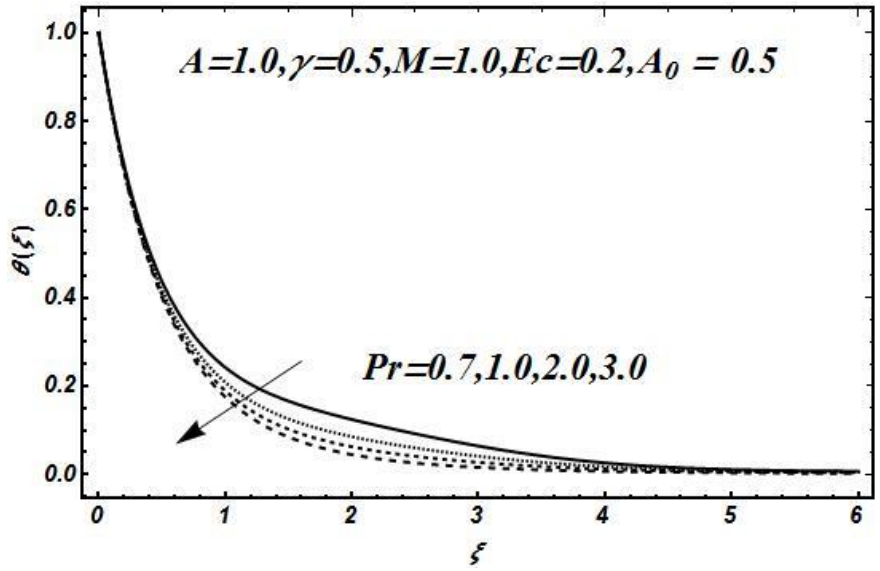

Fig. 3.4. a. Effects of the Prandtl number Pr on the $\theta(\xi)$.

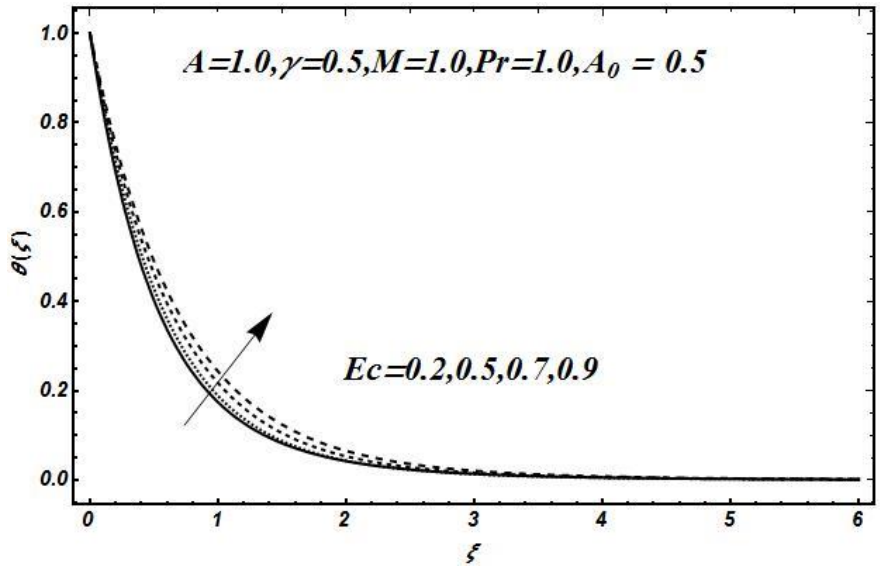

Fig. 3.4. b. Effects of the Eckert number Ec on the $\theta(\xi)$.

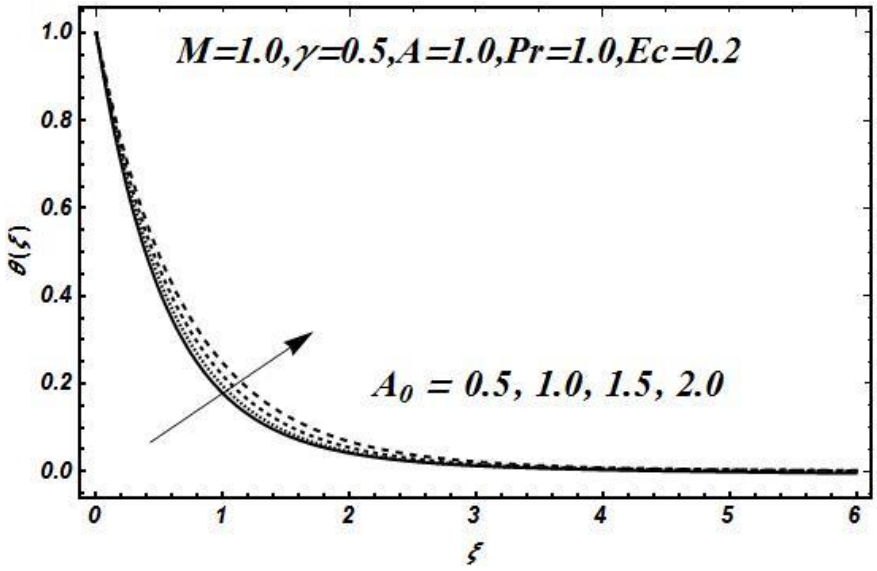

Fig. 3.4. c. Effects of the temperature exponent A_0 on the $\theta(\xi)$.

CHAPTER 4

Investigation of Unsteady Flow of Micropolar Fluid over an Exponentially Stretching Sheet

4.1 Introduction

The unsteady hydromagnetic flow of a micropolar fluid over an exponentially stretched sheet is investigated in this work. The homotopy analysis method (HAM) is utilized to solve the system of non-linear differential equations that arises from the governing partial differential equations based on the related similarity variables. A brief explanation of the physical characteristics impacting the flow and transfer of heat phenomena is given using tables and figures. A comparison with the published literature serves as validation for the current study.

4.2 Mathematical Formulation

The Micropolar fluid phenomenon is considered when an incompressible fluid with viscosity is flowing over a sheet that is being stretched exponentially in x direction. Applying a normal magnetic field with strength $B(x,t) = \frac{B_\circ}{\sqrt{(1-ct)}} e^{x/L}$ on the surface where B_0 is the stable. Here, L denotes the length and c denotes the dimensional constant. Because of the magnetic Reynolds number is minimal the effects of the induced magnetic field are ignored. While the surface is being extended with an exponential velocity $U_w(x,t) = \frac{U_\circ}{(1-ct)} e^{x/L}$, the surface temperature is kept at $T_w(x) = T_\infty + \frac{T_\circ}{(1-ct)} e^{x/2L}$. The ambient temperature of the fluid is taken to be T_∞. The entire treatment is based on boundary layer assumptions. The velocity pattern of the boundary layer flow can be shown as follows:

$$\boldsymbol{V} = [u(x,y), v(x,y), 0]. \tag{4.1}$$

The equations of motion for micropolar unsteady flow defined as below;

$$\boldsymbol{\nabla}.\boldsymbol{V} = 0\,, \tag{4.2}$$

$$\rho\frac{dV}{dt} + \rho(\boldsymbol{V}\cdot\boldsymbol{\nabla})\boldsymbol{V} = -\boldsymbol{\nabla}P + \kappa(\boldsymbol{\nabla}\times\mathbf{N}) - (\mu+\kappa)\boldsymbol{\nabla}\times(\boldsymbol{\nabla}\times\boldsymbol{V}) + (\boldsymbol{J}\times\boldsymbol{B})\,, \tag{4.3}$$

$$\rho_j\frac{dN}{dt} + \rho j(\boldsymbol{V}.\boldsymbol{\nabla})\boldsymbol{N} = (\alpha+\beta+\gamma)\boldsymbol{\nabla}(\boldsymbol{\nabla}.\boldsymbol{N}) - \gamma\boldsymbol{\nabla}\times(\boldsymbol{\nabla}\times\boldsymbol{N}) + \kappa(\boldsymbol{\nabla}.\mathbf{V}) - 2\kappa\boldsymbol{N}\,, \tag{4.4}$$

$$\rho c_p\frac{dT}{dt} = -\mathrm{div}\mathbf{q} + \boldsymbol{\tau}.\mathbf{L}\,, \tag{4.5}$$

where

$$\boldsymbol{q} = -kgradT\,. \tag{4.6}$$

The Cauchy stress tensor $\boldsymbol{\tau}$ is defined as:

$$\boldsymbol{\tau} = -p\boldsymbol{I} + \mu\boldsymbol{A_1}\,, \tag{4.7}$$

In this ρ is density of fluid, c_p is specific heat capacity, $\frac{d}{dt}$ is material derivative, **L** is velocity gradient, k is thermal conductivity, q is heat flux, T is the fluid temperature, V is velocity profile, j is electric current density and $\boldsymbol{A_1}$ first Rivilin-Erickson tensor which is given by:

$$\boldsymbol{A_1} = \boldsymbol{L} + \boldsymbol{L}^T\,. \tag{4.8}$$

Using Eq. (4.1), we obtain

$$\boldsymbol{L} = grad\,\boldsymbol{V} = \begin{bmatrix} \frac{\partial u}{\partial x} & \frac{\partial u}{\partial y} & 0 \\ \frac{\partial v}{\partial x} & \frac{\partial v}{\partial y} & 0 \\ 0 & 0 & 0 \end{bmatrix} \text{and } \boldsymbol{L}^T = (grad\,\boldsymbol{V})^T = \begin{bmatrix} \frac{\partial u}{\partial x} & \frac{\partial v}{\partial x} & 0 \\ \frac{\partial u}{\partial y} & \frac{\partial v}{\partial y} & 0 \\ 0 & 0 & 0 \end{bmatrix}, \tag{4.9}$$

$$\boldsymbol{A_1} = \begin{bmatrix} 2\frac{\partial u}{\partial x} & \frac{\partial u}{\partial y}+\frac{\partial v}{\partial x} & 0 \\ \frac{\partial v}{\partial x}+\frac{\partial u}{\partial y} & 2\frac{\partial v}{\partial y} & 0 \\ 0 & 0 & 0 \end{bmatrix}. \tag{4.10}$$

The component form of governing equation is defined below;

$$\frac{\partial u}{\partial x}+\frac{\partial v}{\partial y}=0\,, \tag{4.11}$$

$$\frac{\partial u}{\partial t}+u\frac{\partial u}{\partial x}+v\frac{\partial u}{\partial y}=\left(\frac{\mu+\kappa}{\rho}\right)\frac{\partial^2 u}{\partial y^2}+\frac{k}{\rho}\frac{\partial N}{\partial y}-\frac{\sigma {B_0}^2}{\rho}u\,, \tag{4.12}$$

$$\rho j\left(\frac{\partial N}{\partial t}+u\frac{\partial N}{\partial x}+v\frac{\partial N}{\partial y}\right)=\gamma^*\frac{\partial^2 N}{\partial y^2}-k\left(2N+\frac{\partial u}{\partial y}\right), \tag{4.13}$$

$$\frac{\partial T}{\partial t}+u\frac{\partial T}{\partial x}+v\frac{\partial T}{\partial y}=\alpha\frac{\partial^2 T}{\partial y^2}+\left(\frac{\mu+\kappa}{\rho c_p}\right)\left(\frac{\partial u}{\partial y}\right)^2. \tag{4.14}$$

The appropriate boundary conditions are;

$$\left.\begin{array}{c} u=u_w(x,t)=\frac{U_0}{(1-ct)}e^{\frac{x}{L}}, v=0, T=T_w(x,t)=T_\infty+\frac{T_0}{(1-ct)^2}e^{\frac{nx}{2L}}\ at\ y=0,\\ N=-n_0\left(\frac{\partial u}{\partial y}\right), at\ y=0,\\ u\to 0, N\to 0, T\to T_\infty\ at\ y\to\infty, \end{array}\right\} \tag{4.15}$$

Here, the velocity components in the (x, y) directions are denoted by (u, v), respectively. The variables T, N, j, ρ, k, σ and c_p denotes temperature, micro-rotation vector, micro inertia, fluids density, thermal conductivity, electrical conductivity and specific heat at constant pressure, respectively. T_∞ is the temperature for away from the surface, while T_0 is the reference temperature. The reference velocity is U_0 and c is the constant with $ct < 1$.

The non dimensionalised Eqs. (4.11)-(4.14) are solved using these similarity transformations;

$$\left.\begin{array}{cc} u=\frac{U_0}{1-ct}e^{x/L}f'(\xi), v=-\sqrt{\frac{U_0\nu}{2L(1-ct)}}e^{x/2L}[f(\xi)+\xi f'(\xi)], & \xi=\sqrt{\frac{U_0}{2\nu(1-ct)}}e^{x/2L}y,\\ N=\frac{U_0}{(1-ct)}\sqrt{\frac{U_0}{2\nu L(1-ct)}}e^{3x/2L}h(\xi), & \theta(\xi)=\frac{T-T_\infty}{T_w-T_\infty}. \end{array}\right\} \tag{4.16}$$

By substituting Eq. (4.16) into Eqs. (4.11)-(4.14), the continuity Eq. (4.11) is identically satisfied, and Eqs. (4.12), (4.13) and (4.14) take the following form:

$$f''' + ff'' - 2f'^2 - A(\xi f'' + 2f') + kh' - Mf' = 0, \tag{4.17}$$

$$\left(1 + \frac{k}{2}\right)h'' - A\left[\frac{3}{2}h + \frac{1}{2}\xi h'\right] - 3f'h + fh' + kA_1[2h + f''] = 0, \tag{4.18}$$

$$\theta'' + Pr[f\theta' - f'\theta] - APr[4\theta + \xi\theta'] + (1 + k)PrEcf''^2 = 0, \tag{4.19}$$

After applying Eq. (4.16) the related boundary conditions are

$$\left.\begin{array}{c} f(0) = 0, f'(0) = 1, h(0) = -N_0 f''(0), \theta(0) = 1, \\ f'(\xi) \to 0, h(\xi) \to 0, \theta(\xi) \to 0 \; as \; \xi \to \infty. \end{array}\right\} \tag{4.20}$$

Here, $A = \frac{CLe^{-X}}{U_0}$ is the unsteadiness parameter, $M = \frac{2\sigma {B_0}^2 L}{\rho U_0}$ denotes the magnetic field parameter, $X = \frac{x}{L}$ is the dimensionless parameter, $Pr = \frac{uC_p}{k}$ is the prandtl number, $\gamma = \alpha\sqrt{\frac{U_0 e^X}{2VL(1-ct)}}$ is slip parameter, and $Ec = \frac{{U_w}^2}{C_p(T_w - T_\infty)}$ is the Eckert number and $A_1 = \frac{CLe^{-X}(1-ct)}{U_0}$ is a dimensionless parameter. The local Nusselt number Nu_x and the skin friction coefficient Cf_x are described as:

$$Cf_x = \frac{\tau_w|_{y=o}}{\rho {u^2}_w}, \qquad Nu_x = \frac{xq_w|_{y=o}}{k((T_w - T_\infty))}, \tag{4.21}$$

where the heat flux q_w at the surface and the shear stress τ_w are explained as:

$$\tau_w = [(\mu + k))\left(\frac{\partial u}{\partial y}\right) + kN]\Big|_{y=0}, \qquad q_w = -k\left(\frac{\partial T}{\partial y}\right)\Big|_{y=0}. \tag{4.22}$$

The local Nusselt number Nu_x and the dimensionless form of the skin friction coefficient Cf_x can be retrieved by using Eq. (4.16) and putting Eq. (4.22) into Eq. (4.21):

$${Re_x}^{1/2} Cf_x = [1 + (1 - N_0)K]f''(0), \qquad \sqrt{\frac{2}{X}}{Re_x}^{1/2} Nu_x = -\theta'(0), \tag{4.23}$$

where $Re_x = \frac{U_w x}{v}$ is the local Reynolds number.

4.3 Homotopic Solution

The HAM is an analytical methodology that is useful for solving high nonlinear equations. This technique has been used to solve heat transport and fluid dynamics problems. The homotopy analysis method in this article solved Eqs. (4.17), (4.18) and (4.19) by considering the following linear operators with linear guesses, using the boundary conditions from Eq. (4.20):

$$\left.\begin{aligned} f_0(\xi) &= \tfrac{1}{1+\gamma}\left(1 - e^{-\xi}\right), \\ h_0(\xi) &= n_0 e^{-\xi}, \\ \theta_0(\xi) &= e^{-\xi}. \end{aligned}\right\} \tag{4.24}$$

and

$$\left.\begin{aligned} \mathcal{L}_f(f) &= \frac{d^3 f}{d\xi^3} - \frac{df}{d\xi}, \\ \mathcal{L}_h(h) &= \frac{d^2 h}{d\xi^2} - h, \\ \mathcal{L}_\theta(\theta) &= \frac{d^2 \theta}{d\xi^2} - \theta. \end{aligned}\right\} \tag{4.25}$$

The following attributes belong to the operator mentioned above:

$$\left.\begin{aligned} \mathcal{L}_f\left(S_1 + S_2 e^{\xi} + S_3 e^{-\xi}\right) &= 0, \\ \mathcal{L}_h\left(S_4 e^{\xi} + S_5 e^{-\xi}\right) &= 0, \\ \mathcal{L}_\theta\left(S_6 e^{\xi} + S_7 e^{-\xi}\right) &= 0, \end{aligned}\right\} \tag{4.26}$$

where $S_{r'}, (r = 1,2, \ldots 7)$ are arbitrary constants.

The problem of zeroth order deformation can be expressed as follows:

$$(1-q)\mathcal{L}_f[\bar{F}(\xi;q) - f_0(\xi)] = h_f \mathcal{N}_f[\bar{F}(\xi;q)], \tag{4.27}$$

$$(1-q)\mathcal{L}_h[\bar{H}(\xi;q) - h_0(\xi)] = h_h \mathcal{N}_h[\bar{F}(\xi;q), \bar{H}(\xi;q)], \tag{4.28}$$

$$(1-q)\mathcal{L}_\theta[\bar{\Theta}(\xi;q) - \theta_0(\xi)] = h_\theta \mathcal{N}_\theta[\bar{F}(\xi;q), \bar{\Theta}(\xi;q)], \tag{4.29}$$

with

$$\left.\begin{array}{c}\bar{F}(0;q)=0,\frac{\partial\bar{F}(0;q)}{\partial\xi}=1,\bar{H}(0;q)=-n\frac{\partial^2\bar{F}(0;q)}{\partial\xi^2},\bar{\Theta}(0;q)=1,\\ \frac{\partial\bar{F}(\infty;q)}{\partial\xi}=0,\bar{H}(\infty;q)=0,\ \bar{\Theta}(\infty;q)=0.\end{array}\right\} \tag{4.30}$$

In this case, $q\epsilon[0,1]$ indicates the embedding parameter associated with the deformation mappings $\bar{F}(\xi;q)$, $\bar{H}(\xi;q)$, $\bar{\Theta}(\xi;q)$ that continuously deform from $f_0(\xi)$, $h_0(\xi)$, $\theta_0(\xi)$ to $f(\xi)$, $h(\xi)$, $\theta(\xi)$ when q varies from 0 to 1. The convergence control parameters are represented by h_f, h_h and h_θ.

The following defines the nonlinear operators:

$$\left.\begin{array}{c}\mathcal{N}_f[\bar{F}(\xi;q)]=\frac{\partial^3\bar{F}(\xi;q)}{\partial\xi^3}+\bar{F}(\xi;q)\frac{\partial^2\bar{F}(\xi;q)}{\partial\xi^2}-2(\frac{\partial\bar{F}(\xi;q)}{\partial\xi})^2\\ -A\left(\xi\frac{\partial^2\bar{F}(\xi;q)}{\partial\xi^2}+2\frac{\partial\bar{F}(\xi;q)}{\partial\xi}\right)-M\frac{\partial\bar{F}(\xi;q)}{\partial\xi},\end{array}\right\} \tag{4.31}$$

$$\left.\begin{array}{c}\mathcal{N}_h[\bar{F}(\xi;q),\bar{H}(\xi;q)]=\left(1+\frac{k}{2}\right)\frac{\partial^2\bar{H}(\xi;q)}{\partial\xi^2}-A\left[\frac{3}{2}\bar{H}(\xi;q)+\frac{1}{2}\xi\frac{\partial\bar{H}(\xi;q)}{\partial\xi}\right]-3\frac{\partial\bar{F}(\xi;q)}{\partial\xi}\bar{H}(\xi;q)\\ +\bar{F}(\xi;q)\frac{\partial\bar{H}(\xi;q)}{\partial\xi}+A_1k\left(2\bar{H}(\xi;q)+\frac{\partial^2\bar{F}(\xi;q)}{\partial\xi^2}\right),\end{array}\right\} \tag{4.32}$$

$$\left.\begin{array}{c}\mathcal{N}_\theta[\bar{F}(\xi;q),\bar{\Theta}(\xi;q)]=\frac{\partial^2\bar{\Theta}(\xi;q)}{\partial\xi^2}+Pr\bar{F}(\xi;q)\frac{\partial\bar{\Theta}(\xi;q)}{\partial\xi}-A_oPr\frac{\bar{F}(\xi;q)}{\partial\xi}\bar{\Theta}(\xi;q)\\ -APr\left(4\bar{\Theta}(\xi;q)+\xi\frac{\partial\bar{\Theta}(\xi;q)}{\partial\xi}\right)+PrEc\left(\frac{\partial^2\bar{F}(\xi;q)}{\partial\xi^2}\right)^2+MPrEc\left(\frac{\partial\bar{F}(\xi;q)}{\partial\xi}\right),^2\end{array}\right\} \tag{4.33}$$

The literature has the remaining procedure details. With the limitations on the bounds of Eq. (4.20), the solution of the differential Eqs. (4.17), (4.18) and (4.19) can be represented as an infinite series as follows:

$$\left.\begin{array}{l}f(\xi)=f_0(\xi)+\sum_{m=1}^{\infty}f_m(\xi),\\ h(\xi)=h_0(\xi)+\sum_{m=1}^{\infty}h_m(\xi),\\ \theta(\xi)=\theta_0(\xi)+\sum_{m=1}^{\infty}\theta_m(\xi).\end{array}\right\} \tag{4.34}$$

The above procedure makes it clear that the series solutions listed in Eq. (4.34) have convergence control parameters, h_f, h_h and h_θ that can be used to to control rate of convergence of the series solutions.

4.4 Results and Discussions

This part aims to investigate the continuing effects of several parameters related to temperature, velocity, and micro rotation curve fields. Fig.4.1. exhibit the h curve which give the ranges of $-0.1 < h_f < -0.5, -0.2 < h_h < -0.5$, and $-0.2 < h_\theta < -0.5$.

Fig.4.2. explains the effects of variation of M on velocity profile $f'(\xi)$ which displays that the Lorentz force becomes stronger as the magnetic field parameter M is increased, obstructing the fluid's motion and resulting in a decrease in velocity $f'(\xi)$. Furthermore, for a fixed M, the velocity $f'(\xi)$ decreases with increasing distance ξ and becomes asymptotically zero in the distant regime. Fig.4.3. demonstrates the impact of variation of M on temperature distribution $\theta(\xi)$. It is quite evident from the figure that the resistive force becomes greater as the value of M increases which consequently results in grow in the temperature $\theta(\xi)$. Fig.4.4. depicts the variation of magnetic field parameter M on microrotation profile $h(\xi)$. An increase in the microrotation profile $h(\xi)$ is seen with increase in the value of M.

Fig.4.5. illustrates the impact of Prandtl number Pr on temperature profile $\theta(\xi)$. It demonstrates how Pr affects the temperature distribution $\theta(\xi)$. A rise in the value of Pr is associated with a decrease in the thickness of the thermal boundary layer. Fig.4.6. shows that the temperature distribution $\theta(\xi)$ effects enhance when the value of Eckert number Ec is increased. An augmentation in fluid temperature $\theta(\xi)$ is caused by increase in Eckert number Ec. Fig. 4.7. represents the effects of unsteadiness parameter A on velocity profile $f'(\xi)$. The impact of increasing A results in decrease in fluid velocity.

By adjusting the values of the unsteadiness parameter A, Fig.4.8. shows how the fluid temperature $\theta(\xi)$ behaves. Increasing the values of A results in a notable decrease in temperature profile. Fig.4.9. shows an increase in microrotation profile $h(\xi)$ with an increase in micropolar parameter K. The effects of the micropolar parameter K on the velocity profile $f'(\xi)$ are depicted here in Fig.4.10. This figure demonstrates that $f'(\xi)$ increases with increase in the value of K. Furthermore, as K rises, the boundary layer thickness also enhances. Fig. 4.11. shows the impact of the micropolar parameter K on the temperature profile $\theta(\xi)$. The boundary layer's thickness increases together with K. Fig.4.12. indicates variation of micropolar parameter K on microrotation profile $h(\xi)$. Higher the values of micropolar parameter K also causes increase in microrotation profile $h(\xi)$.

Fig.4.13. is plotted to display the effects of variation in N_0 on velocity profile $f'(\xi)$. As the value of N_0 increases, a decrease in velocity profile $f'(\xi)$ is noticed. Fig. 4.14. shows the effects of microrotation parameter N_0 on temperature distribution $\theta(\xi)$. It is observed that raising the value microrotation parameter N_0 led to a corresponding rise in $\theta(\xi)$. An increase in microrotation profile $h(\xi)$ is witnessed with an increase in microrotanion parameter N_0 as shown in Fig. 4.15. The impact of change in dimensionless parameter A_1 on temperature distribution $\theta(\xi)$ is displayed in Fig.4.16. For higher values of the unsteadiness parameter A_1, the temperature distribution $\theta(\xi)$ is also high.

The purpose of Table. 4.1. is to display the effects of the parameters K, A, and M on the dimensionless skin friction coefficient $-[1+(1-N_0)K]f''(0)$ using HAM method. This demonstrates that an increase in the value of M, K and A increases the skin friction coefficient at the surface. For various values of the parameters K, M, A, A_1, and N_0, the values of $h'(0)$ were determined using the HAM technique, as shown in Table. 4.2. which determined that the parameters M, A, N_0 increases and A_1 and K decreases. In Table. 4.3. the values of $-\theta'(0)$ were found using the HAM approach for different values of the parameters K, M, A, Pr, Ec, N_0, and A_1. The value of $-\theta'(0)$ increases the microrotation parameter N_0, the unsteadiness parameter A, and the Prandtl number Pr. Conversely, there was a decrease in the effect on $-\theta'(0)$ when the parameters M, K, A_1 and Ec were increased.

Table. 4.1. Numerical values of $-[1+(1-N_0)K]f''(0)$ that were obtained by the HAM for variation in the values of magnetic field parameter M, the unsteadiness parameter A, and the micropolar parameter K.

K	A	M	$-[1+(1-N_0)K]f''(0)$
1.0	1.0	1.0	2.40988
		2.0	2.66933
		3.0	2.996539
1.0	0.5	1.0	2.409883
	1.0		2.6794335
	1.5		2.9216325
0.5	0.5	1.0	2.0082362
1.0			2.2377615
1.5			2.38975275

Table. 4.2. Numerical ideals of $h'(0)$ that were obtained by the homotopy analysis technique (HAM) for variation in the values of micropolar parameter K, the magnetic field parameter M, and the unsteadiness parameter A, the dimensionless parameter A_1, and microrotation parameter N_0.

K	M	A	A_1	N_0	$h'(0)$
1.0	1.0	1.0	1.0	1.0	1.640265
				2.0	1.77182
				3.0	2.274809
1.0	1.0	1.0	1.0	1.0	1.1357827
			2.0		0.1989345
			3.0		0.2228381
1.0	1.0	0.5	1.0	1.0	1.740472
		1.0			2.381722
		1.5			3.083988
1.0	1.0	0.5	1.0	1.0	1.422461
	2.0				1.740472
	3.0				2.164271
0.5	1.0	1.0	1.0	1.0	1.083988
1.0					0.994930
1.5					0.549571

Table. 4.3. Numerical values of $-\theta'(0)$ that were obtained by the HAM technique for variation in the values of micropolar parameter K, the magnetic field parameter M, and the unsteadiness parameter A, the dimensionless parameter A_1, and microrotation parameter N_0, the Prandtl number Pr, and the Eckert number Ec.

K	M	A	A_1	N_0	Pr	Ec	$-\theta'(0)$
1.0	1.0	1.0	1.0	1.0	1.0	1.0	1.715985
						2.0	1.447973
						3.0	1.035826
1.0	1.0	1.0	1.0	1.0	0.7	1.0	1.571012
					1.0		1.715985
					2.0		2.314394
1.0	1.0	1.0	1.0	1.0	0.7	1.0	1.571012
				2.0			2.291414
				3.0			3.035826
1.0	1.0	1.0	1.0	1.0	0.7	1.0	1.135782
			2.0				0.655063
			3.0				0.458196
1.0	1.0	0.5	1.0	1.0	0.7	1.0	1.509092
		1.0					1.980355
		1.5					2.356859
1.0	1.0	0.5	1.0	1.0	0.7	1.0	2.307341
	2.0						1.509092
	3.0						1.426114
0.5	1.0	0.5	1.0	1.0	0.7	1.0	2.35685 9
1.0							1.475677
1.5							1.445671

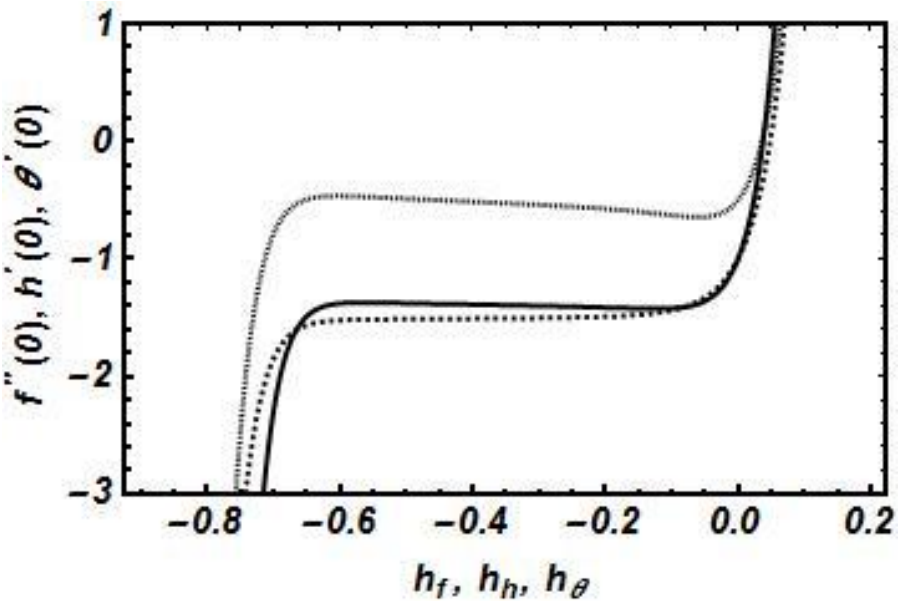

Fig.4.1. The h curve graph

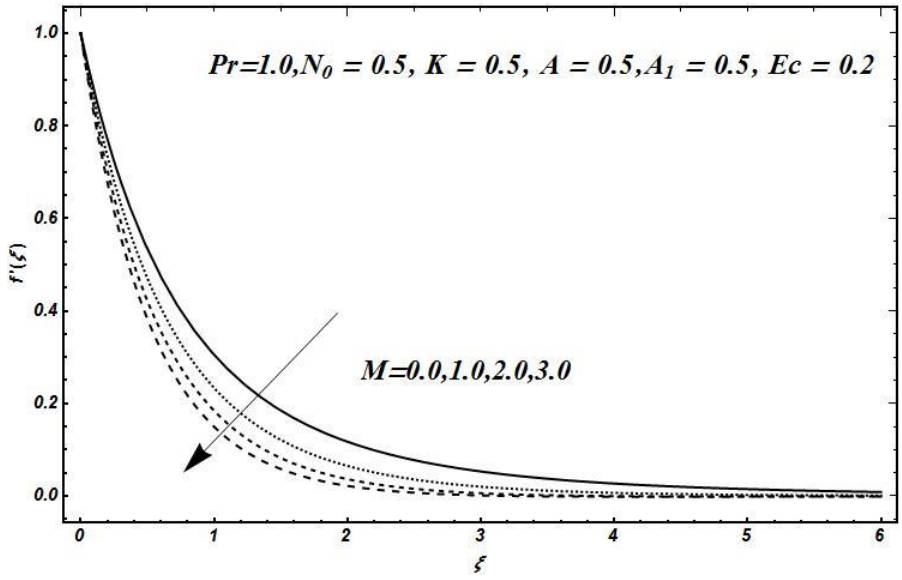

Fig.4.2. Variation of M on $f'(\xi)$.

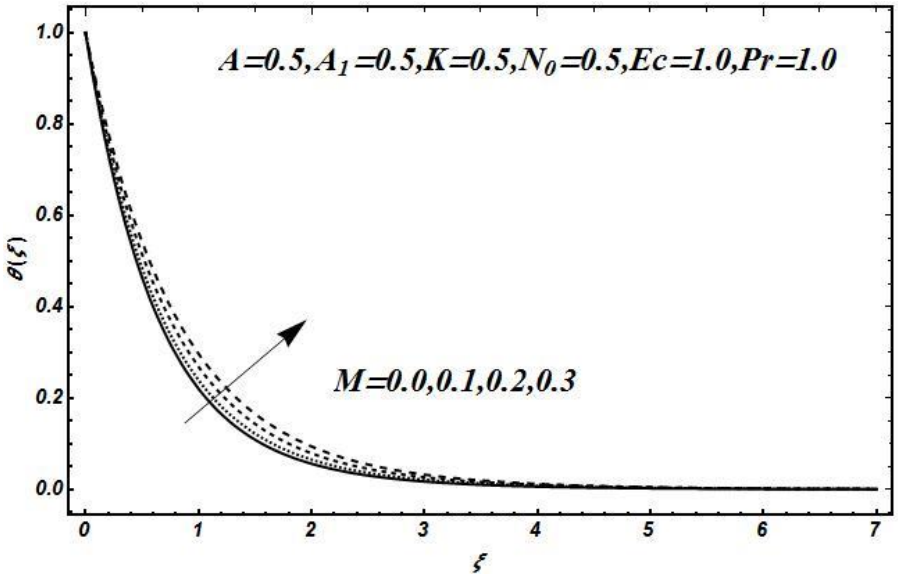

Fig.4.3. Variation of M on $\theta(\xi)$.

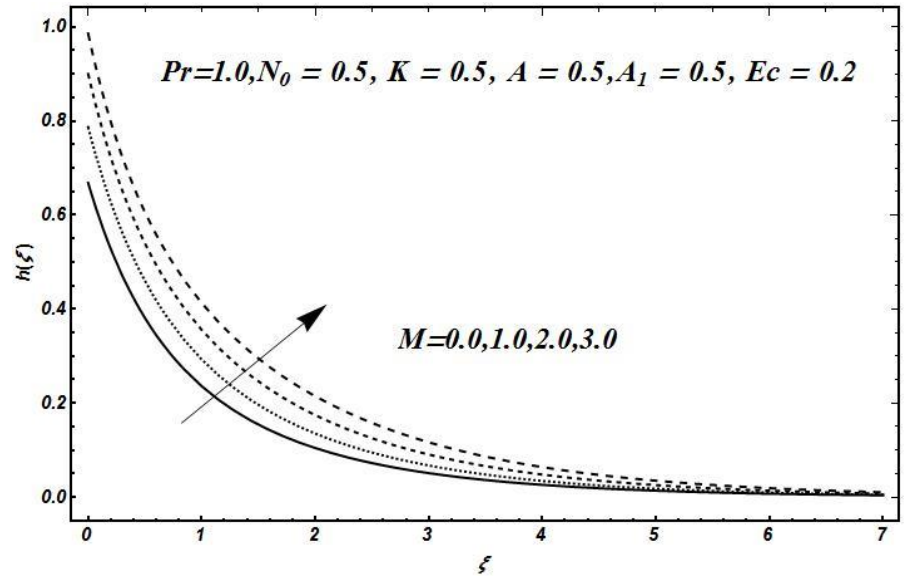

Fig.4.4. Variation of M on $h(\xi)$.

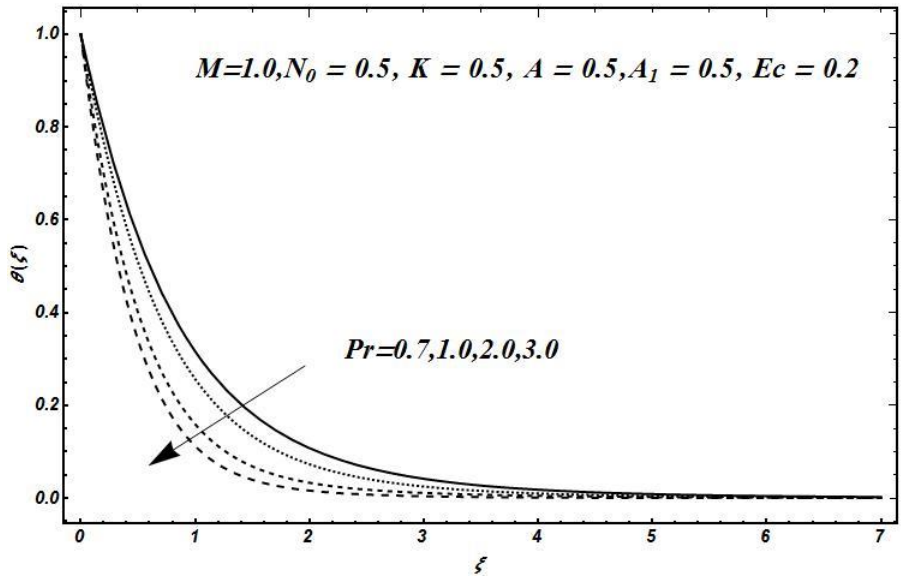

Fig.4.5. Variation of Pr on $\theta(\xi)$.

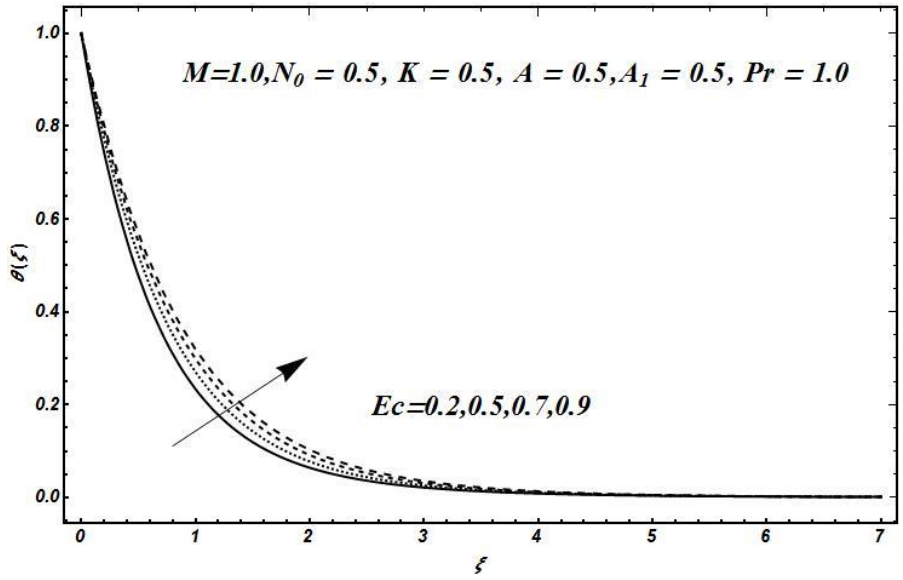

Fig.4.6. Variation of Ec on $\theta(\xi)$.

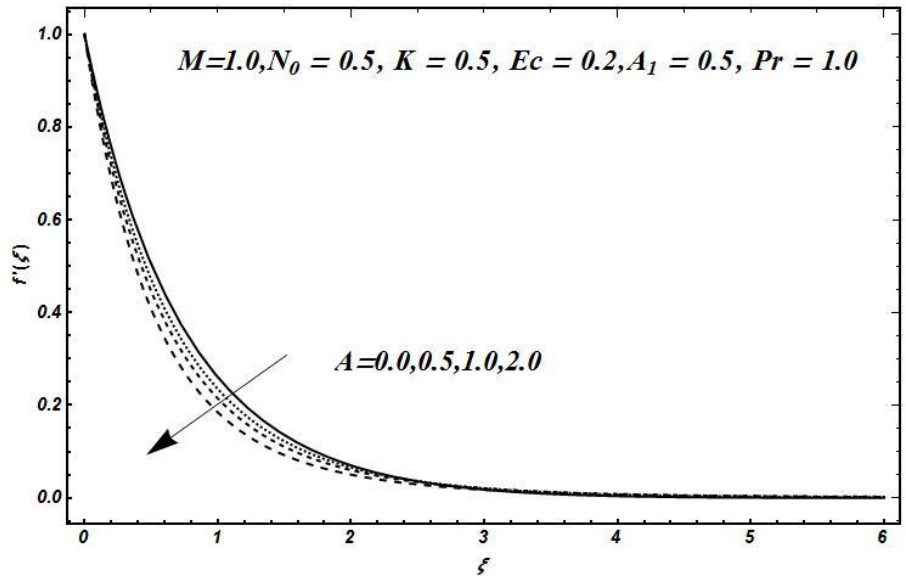

Fig.4.7. Variation of A on $f^{'}(\xi)$.

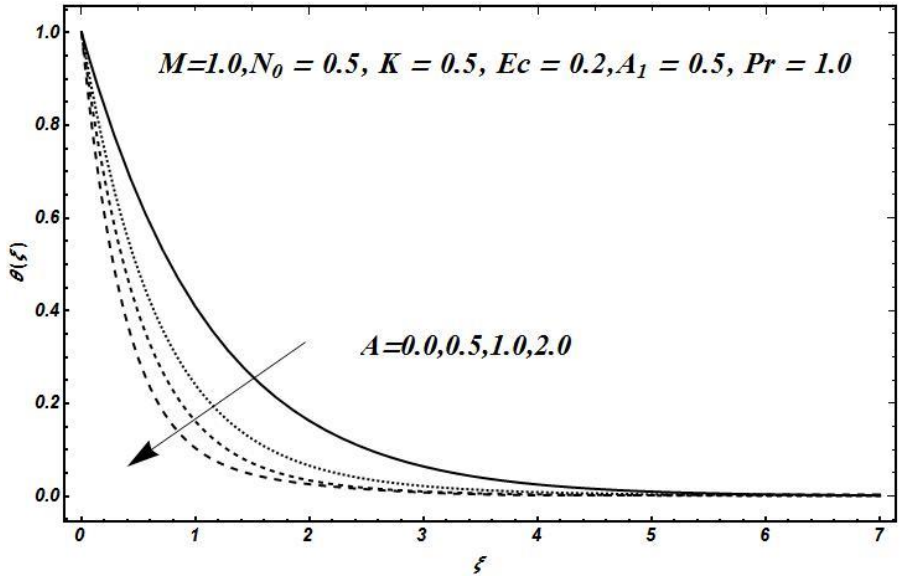

Fig.4.8. Variation of A on $\theta(\xi)$.

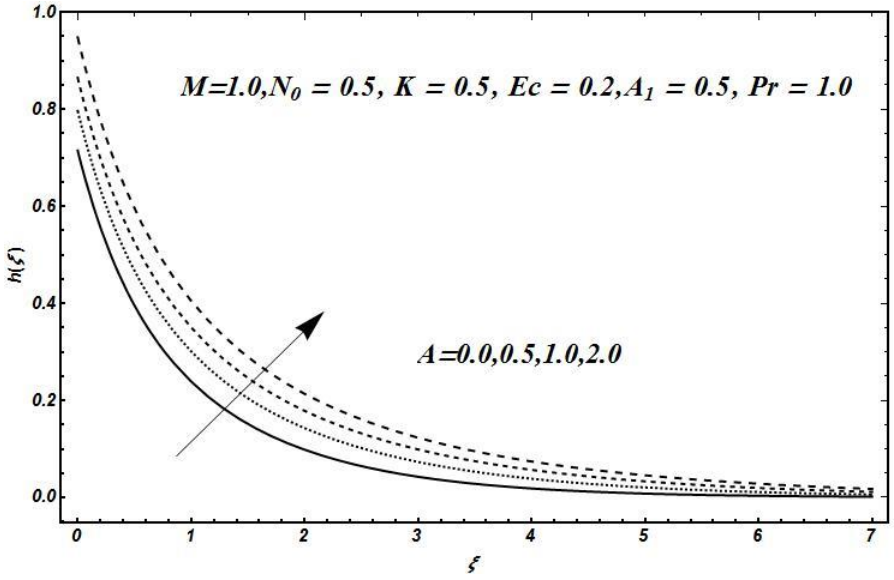

Fig.4.9. Variation of A on $h(\xi)$.

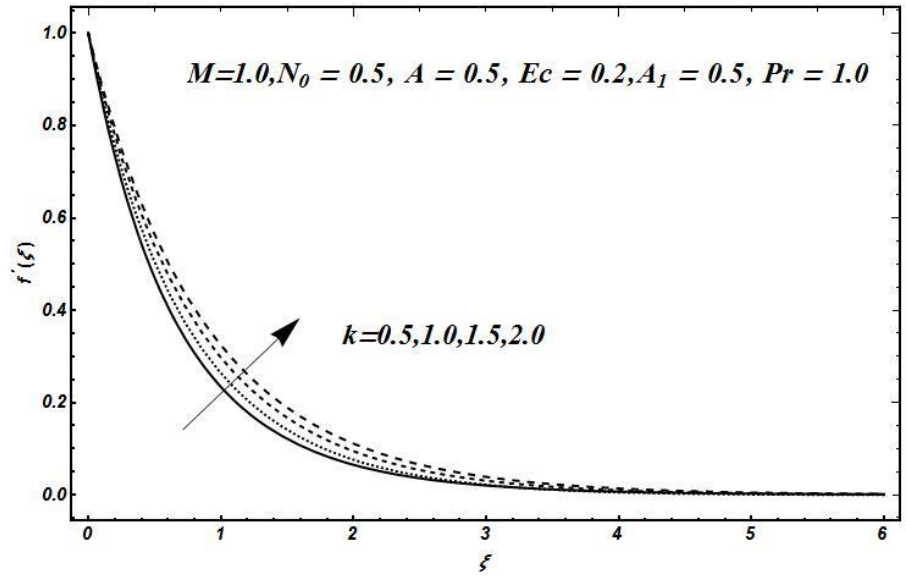

Fig.4.10. Variation of K on $f'(\xi)$.

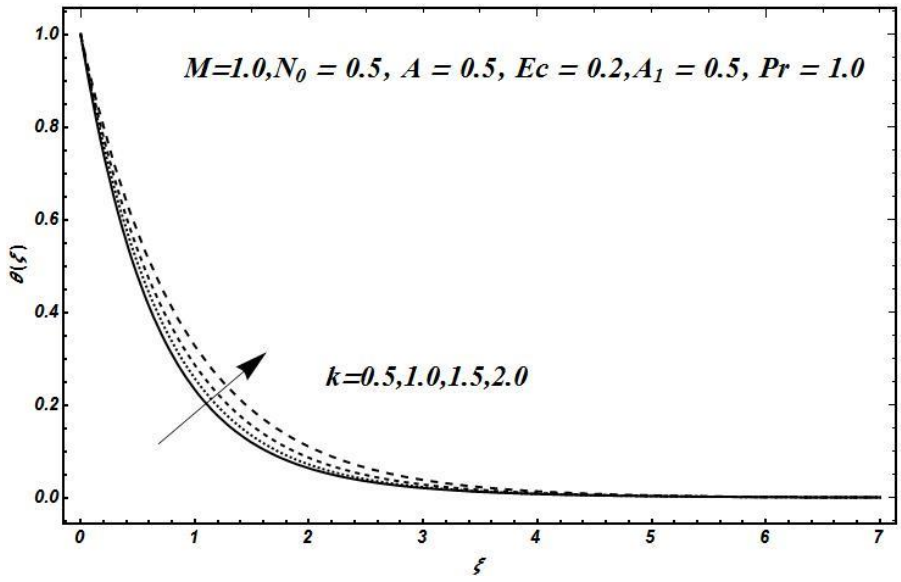

Fig.4.11. Variation of K on $\theta(\xi)$.

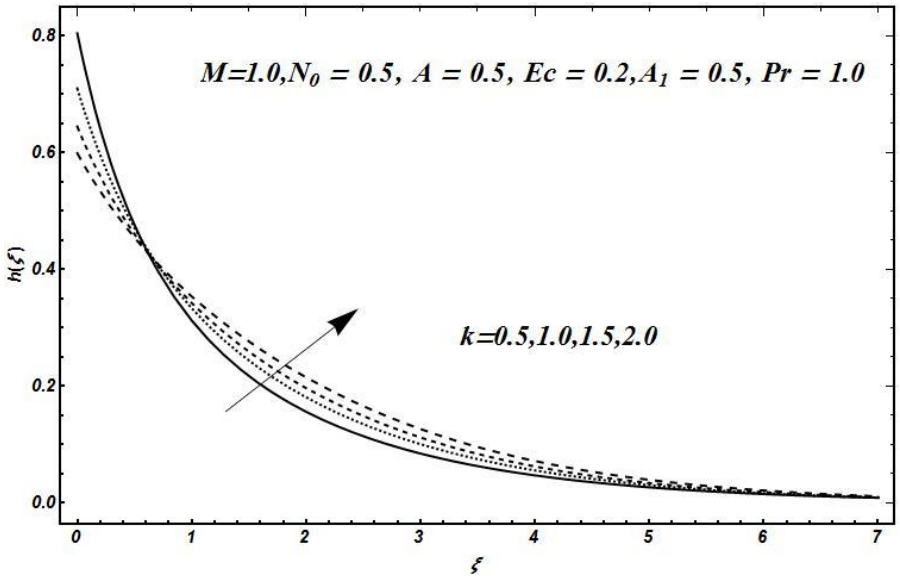

Fig.4.12. Variation of K on $h(\xi)$.

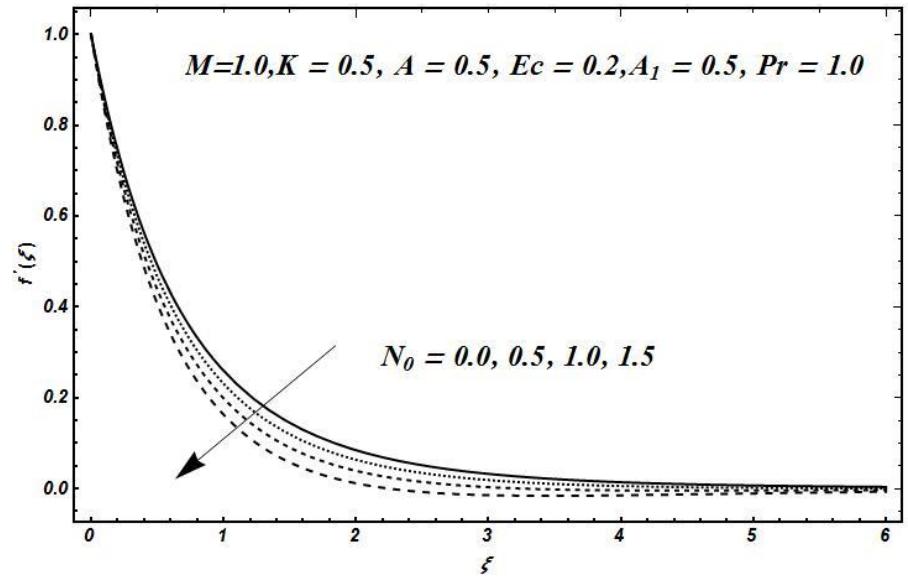

Fig.4.13. Variation of N_0 on $f^{'}(\xi)$.

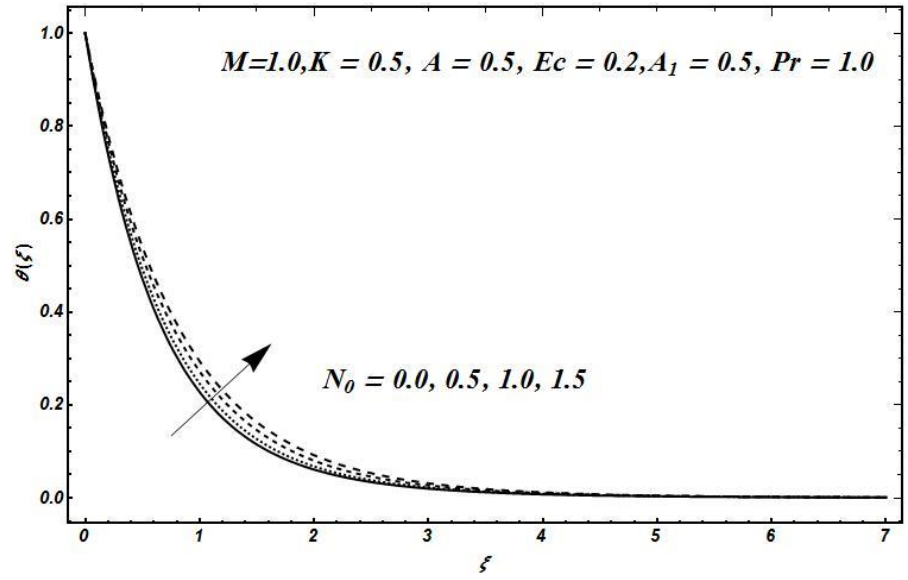

Fig.4.14. Variation of N_0 on $\theta(\xi)$.

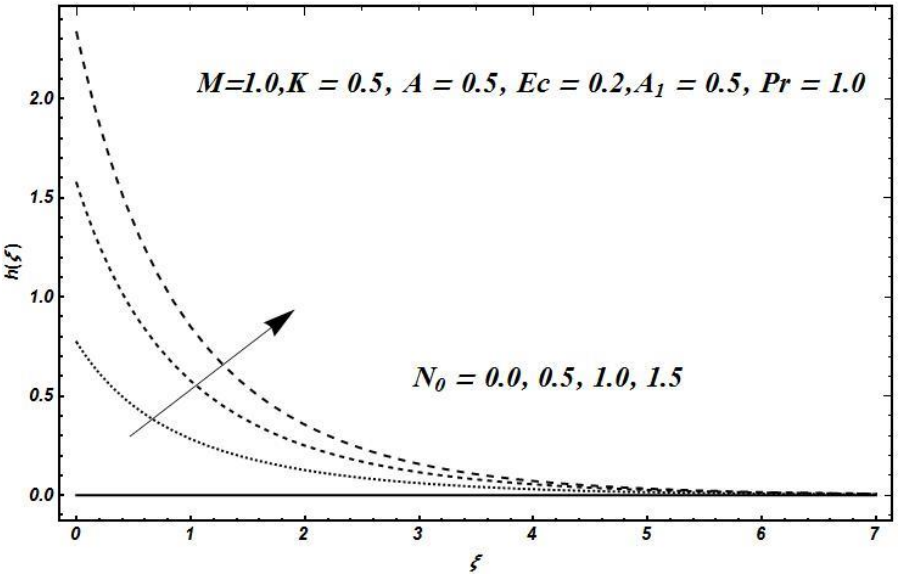

Fig.4.15. Variation of N_0 on $h(\xi)$.

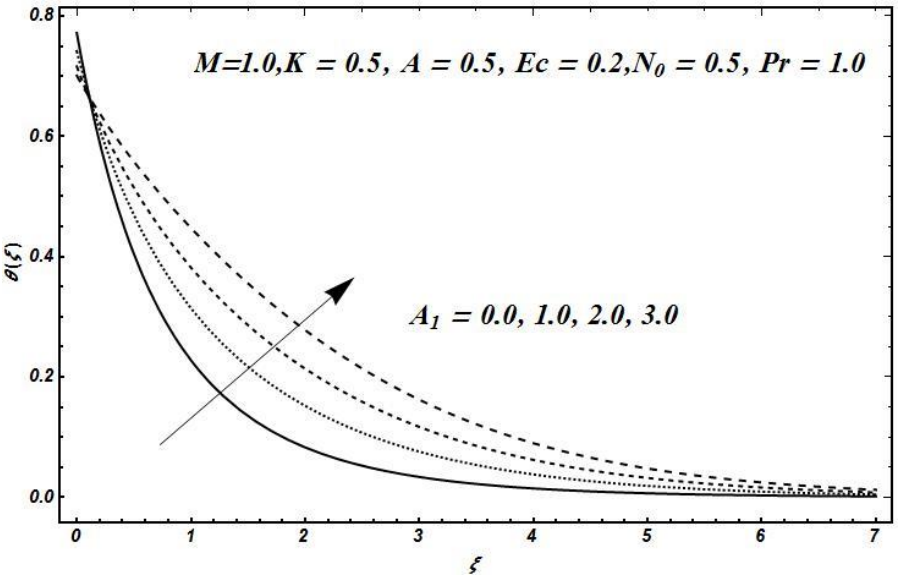

Fig.4.16. Variation of A_1 on $\theta(\xi)$.

CHAPTER 5

CONCLUSION AND FUTURE WORK

5.1 Conclusions

We have investigated the unsteady flow of micropolar fluid over an exponentially stretching sheet. Using the similarity transformations the system of nonlinear partial differential equations converted into nonlinear ordinary differential equations. The HAM technique is used to solve the issue, and the results are briefly reviewed. The unsteady stretched surface, causes the flow behavior. The primary findings are described below:

- The velocity profile $f^{'}$ is decreasing function of M, A, N_0 and increasing function of K.
- The temperature profile has increasing effect on Ec, M, A_1, N_0 and K.
- An increase in Pr and A lowers the temperature as well as the thickness of the thermal boundary layer.
- When N_0, M, A and K is raised, the microrotation profile also increased.
- The skin friction coefficient values decrease as the boundary parameter values increase.

5.2 Future Work

Future research could explore various interesting directions in the area of unsteady flow of micropolar fluid across an exponentially stretched sheet. Initially, the research can be extended to investigate the behaviors and properties of various different types of fluids under diverse conditions. Furthermore, a deeper analysis of the flow behavior under various parameter conditions would be possible by investigating numerical simulations using advanced computational techniques like the Finite Element Method (FEM). Finally, in order to confirm the model's accuracy and applicability in real-world situations, experimental validation of theoretical predictions is important.

REFERENCES

[1] Eringen, A. Cemal, "Theory of micropolar fluids." Journal of mathematics and Mechanics (1966): 1-18.

[2] Shamshuddin, M. D., T. Thirupathi, and P. V. Satya Narayana, "Micropolar fluid flow induced due to a stretching sheet with heat source/sink and surface heat flux boundary condition effects." Journal of Applied and Computational Mechanics 5, no. 5 (2019): 816-826.

[3] Yasmin, Asia, K. Ali, and M. Ashraf, "Study of heat and mass transfer in MHD flow of micropolar fluid over a curved stretching sheet." Scientific reports 10, no. 1 (2020): 4581.

[4] Mandal, I. Chandra, S. Mukhopadhyay, and K. Vajravelu, "Melting heat transfer of MHD micropolar fluid flow past an exponentially stretching sheet with slip and thermal radiation." International Journal of Applied and Computational Mathematics 7 (2021): 1-18.

[5] Patel, R. Harshad, D. S. Patel, and R. Darji, "Mathematical Study of unsteady micropolar fluid flow due to non-linear stretched sheet in the presence of magnetic field." International Journal of Thermofluids 16 (2022): 100232.

[6] Sharma, Surbhi, A. Dadheech, A. Parmar, J. Arora, Q. Al-Mdallal, and S. Saranya, "MHD micro polar fluid flow over a stretching surface with melting and slip effect." Scientific reports 13, no. 1 (2023): 10715.

[7] Fatunmbi, E. O., A. T. Adeosun, and S. S. Okoya. "Entropy generation analysis in an unsteady hydromagnetic micropolar fluid flow along an exponentially stretchable sheet with slip properties." International Journal of Modelling and Simulation 43, no. 4 (2023): 491-506.

[8] Meenakumari, Ramamoorthy, G. Sucharitha, P. Lakshminarayana, and K. Vajravelu, "Darcy-forchheimer flow of a conducting micropolar fluid at a stretching sheet with connective boundary conditions." Journal of Porous Media 27 (2024).

[9] Rajagopal, R. Kumbakonam, T. Y. Na, and A. S. Gupta, "Flow of a viscoelastic fluid over a stretching sheet." Rheologica Acta 23 (1984): 213-215.

[10] Kumaran, V., and G. Ramanaiah, "A note on the flow over a stretching sheet." Acta Mechanica 116, no. 1 (1996): 229-233.

[11] Hamid, M., M. Usman, Z. H. Khan, R. Ahmad, and W. Wang, "Dual solutions and stability analysis of flow and heat transfer of Casson fluid over a stretching sheet." Physics Letters A 383, no. 20 (2019): 2400-2408.

[12] Srinivasulu, Thadakamalla, and B. Shankar Goud, "Effect of inclined magnetic field on flow, heat and mass transfer of Williamson nanofluid over a stretching sheet." Case Studies in Thermal Engineering 23 (2021): 100819.

[13] Alzahrani, Jawaher, H. Vaidya, K. V. Prasad, C. Rajashekhar, D. L. Mahendra, and I. Tlili, "Micro-polar fluid flow over a unique form of vertical stretching sheet: Special emphasis to temperature-dependent properties." Case Studies in Thermal Engineering 34 (2022): 102037.

[14] Ram, M. Sunder, K. Spandana, M. D. Shamshuddin, and S. O. Salawu, "Mixed convective heat and mass transfer in magnetized micropolar fluid flow toward stagnation point on a porous stretching sheet with heat source/sink and variable species reaction." International Journal of Modelling and Simulation 43, no. 5 (2023): 670-682.

[15] Ali, Liaqat, P. Kumar, Z. Iqbal, Sharifah E. Alhazmi, S. Areekara, M. M. Alqarni, A. Mathew, and R. Apsari, "The optimization of heat transfer in thermally convective micropolar-based nanofluid flow by the influence of nanoparticle's diameter and nanolayer via stretching sheet: sensitivity analysis approach." Journal of Non-Equilibrium Thermodynamics 48, no. 3 (2023): 313-330.

[16] Saidulu, B., and K. Sreeram Reddy, "Evaluation of combined heat and mass transfer in hydromagnetic micropolar flow along a stretching sheet when viscous dissipation and chemical reaction is present." Partial Differential Equations in Applied Mathematics 7 (2023): 100467.

[17] Magyari, E., and B. Keller, "Heat and mass transfer in the boundary layers on an exponentially stretching continuous surface." Journal of Physics D: Applied Physics 32, no. 5 (1999): 577.

[18] Bidin, Biliana, and R. Nazar, "Numerical solution of the boundary layer flow over an exponentially stretching sheet with thermal radiation." European journal of scientific research 33, no. 4 (2009): 710-717.

[19] Ishak, and Anuar. "MHD boundary layer flow due to an exponentially stretching sheet with radiation effect." Sains Malaysiana 40, no. 4 (2011): 391-395.

[20] A. El-Aziz, Mohamed, "Viscous dissipation effect on mixed convection flow of a micropolar fluid over an exponentially stretching sheet." Canadian Journal of Physics 87, no. 4 (2009): 359-368.

[21] Awan, A. Ullah, A. A. Akbar, H. Hamam, F. Gamaoun, E. M. Tag-eidin, and A. Abdulrahman, "Characterization of the induced magnetic field on third-grade micropolar fluid flow across an exponentially stretched sheet." Frontiers in Physics 10 (2022): 964653.

[22] Guedri, Kamel, N. A. Ahammad, S. Nadeem, E. M. Tag-eidin, A. U. Awan, and M. F. Yassen, "Insight into the heat transfer of third-grade micropolar fluid over an exponentially stretched surface." Scientific Reports 12, no. 1 (2022): 15577.

[23] Fatunmbi, Ephesus O., S. O. Salawu, and A. Adeniyan. "Buoyancy force and slip conditions on hydromagnetic dissipative flow of micropolar fluid passing an exponentially stretching sheet." Computational Thermal Sciences: An International Journal 14, no. 1 (2022)

[24] A. Khan, Aamir, M. N. Khan, N. A. Ahammad, M. Ashraf, K. Guedri, and A. M. Galal. "Flow investigation of second grade micropolar nanofluid with porous medium over an exponentially stretching sheet." Journal of Applied Biomaterials & Functional Materials 20 (2022): 22808000221089782.

[25] Bakar, F. N. Abu, and S. K. Soid. "MHD Stagnation-Point Flow and Heat Transfer in a Micropolar Fluid over an Exponentially Vertical Sheet." CFD Letters 15, no. 3 (2023): 81-96.

[26] Abbas, Nadeem, M. Ali, W. Shatanawi, and Z. Mustafa. "Thermodynamic properties of Second-grade micropolar nanofluid flow past an exponential curved Riga stretching surface with Cattaneo–Christov double diffusion." Alexandria Engineering Journal 81 (2023): 101-117.

[27] Siddique, Imran, M. Nadeem, R. Ali, and F. Jarad. "Bioconvection of MHD second-grade fluid conveying nanoparticles over an exponentially stretching sheet: A biofuel applications." Arabian Journal for Science and Engineering 48, no. 3 (2023): 3367-3380.

[28] A. El-Aziz, Mohamed. "Radiation effect on the flow and heat transfer over an unsteady stretching sheet." International Communications in Heat and Mass Transfer 36, no. 5 (2009): 521-524.

[29] Khan, Umair, A. Zaib, I. Pop, S. Bakar, and A. Ishak. "Unsteady micropolar hybrid nanofluid flow past a permeable stretching/shrinking vertical plate." Alexandria Engineering Journal 61, no. 12 (2022): 11337-11349.

[30] Kataria, Hari, and M. Mistry. "Effect of Non-linear Radiation on MHD Mixed Convection Flow of a Micropolar fluid Over an Unsteady Stretching Sheet." In Journal of Physics: Conference Series, vol. 1964, no. 2, p. 022005. IOP Publishing, 2021

[31] Abbas, Nadeem, S. Nadeem, and M. N. Khan. "Numerical analysis of unsteady magnetized micropolar fluid flow over a curved surface." Journal of Thermal Analysis and Calorimetry 147, no. 11 (2022): 6449-6459.

[32] Jang, Jaesung, and Seung S. Lee. "Theoretical and experimental study of MHD (magnetohydrodynamic) micropump." Sensors and Actuators A: Physical 80, no. 1 (2000): 84-89.s

[33] Kumar, Anantha, V. Sugunamma, and N. Sandeep. "Numerical exploration of MHD radiative micropolar liquid flow driven by stretching sheet with primary slip: a comparative study." Journal of Non-Equilibrium Thermodynamics 44, no. 2 (2019): 101-122.

[34] Abbas, Amir, H. Ahmad, M. Mumtaz, A. Ilyas, and M. Hussan. "MHD dissipative micropolar fluid flow past stretching sheet with heat generation and slip effects." Waves in Random and Complex Media (2022): 1-15.

[35] Patel, Harshad R., and Snehal D. Patel. "Heat and mass transfer in mixed convection MHD micropolar fluid flow due to non-linear stretched sheet in porous medium with non-uniform heat generation and absorption." Waves in Random and Complex Media (2022): 1-31.

[36] Mahabaleshwar, U. S., A. B. Vishalakshi, and M. Hatami. "MHD micropolar fluid flow over a stretching/shrinking sheet with dissipation of energy and stress work considering mass transpiration and thermal radiation." International Communications in Heat and Mass Transfer 133 (2022): 105966.

[37] Mishra, Pankaj, D. Kumar, Y. D. Reddy, and B. S. Goud. "MHD Williamson micropolar fluid flow pasting a non-linearly stretching sheet under the presence of non linear heat generation/absorption." Journal of the Indian Chemical Society 100, no. 1 (2023): 100845.

[38] Jawad, Muhammad. "A computational study on magnetohydrodynamics stagnation point flow of micropolar fluids with buoyancy and thermal radiation due to a vertical stretching surface." Journal of Nanofluids 12, no. 3 (2023): 759-766.

[39] Bejawada, S. Goud, and M. M. Nandeppanavar. "Effect of thermal radiation on magnetohydrodynamics heat transfer micropolar fluid flow over a vertical moving porous plate." Experimental and Computational Multiphase Flow 5, no. 2 (2023): 149-158.

[40] A. S. Butt, K. Maqbool, S. M. Imran, and A. Babar. "Entropy generation effects in MHD Casson nanofluid past a permeable stretching surface." International Journal of Exergy 31, no. 2 (2020): 150-171.